

Proximal Cerebral Arteries Develop Myogenic Responsiveness in Heart Failure via Tumor Necrosis Factor- α -Dependent Activation of Sphingosine-1-Phosphate Signaling

Jingli Yang, M. Hossein Noyan-Ashraf, Anja Meissner, Julia Voigtlaender-Bolz, Jeffrey T. Kroetsch, Warren Foltz, David Jaffray, Amita Kapoor, Abdul Momen, Scott P. Heximer, Hangjun Zhang, Matthijs van Eede, R. Mark Henkelman, Stephen G. Matthews, Darcy Lidington, Mansoor Husain and Steffen-Sebastian Bolz

Circulation. 2012;126:196-206; originally published online June 5, 2012;
doi: 10.1161/CIRCULATIONAHA.111.039644

Circulation is published by the American Heart Association, 7272 Greenville Avenue, Dallas, TX 75231
Copyright © 2012 American Heart Association, Inc. All rights reserved.
Print ISSN: 0009-7322. Online ISSN: 1524-4539

The online version of this article, along with updated information and services, is located on the World Wide Web at:

<http://circ.ahajournals.org/content/126/2/196>

Data Supplement (unedited) at:

<http://circ.ahajournals.org/content/suppl/2012/06/04/CIRCULATIONAHA.111.039644.DC1.html>

Permissions: Requests for permissions to reproduce figures, tables, or portions of articles originally published in *Circulation* can be obtained via RightsLink, a service of the Copyright Clearance Center, not the Editorial Office. Once the online version of the published article for which permission is being requested is located, click Request Permissions in the middle column of the Web page under Services. Further information about this process is available in the [Permissions and Rights Question and Answer](#) document.

Reprints: Information about reprints can be found online at:
<http://www.lww.com/reprints>

Subscriptions: Information about subscribing to *Circulation* is online at:
<http://circ.ahajournals.org/subscriptions/>

Proximal Cerebral Arteries Develop Myogenic Responsiveness in Heart Failure via Tumor Necrosis Factor- α -Dependent Activation of Sphingosine-1-Phosphate Signaling

Jingli Yang, MD*; M. Hossein Noyan-Ashraf, PhD*; Anja Meissner, PhD*;
Julia Voigtlaender-Bolz, MD; Jeffrey T. Kroetsch, MSc; Warren Foltz, PhD; David Jaffray, PhD;
Amita Kapoor, MSc; Abdul Momen, MD; Scott P. Heximer, PhD; Hangjun Zhang, MD;
Matthijs van Eede, PhD; R. Mark Henkelman, PhD; Stephen G. Matthews, PhD;
Darcy Lidington, PhD; Mansoor Husain, MD*; Steffen-Sebastian Bolz, MD, PhD*

Background—Heart failure is associated with neurological deficits, including cognitive dysfunction. However, the molecular mechanisms underlying reduced cerebral blood flow in the early stages of heart failure, particularly when blood pressure is minimally affected, are not known.

Methods and Results—Using a myocardial infarction model in mice, we demonstrate a tumor necrosis factor- α (TNF α)-dependent enhancement of posterior cerebral artery tone that reduces cerebral blood flow before any overt changes in brain structure and function. TNF α expression is increased in mouse posterior cerebral artery smooth muscle cells at 6 weeks after myocardial infarction. Coordinately, isolated posterior cerebral arteries display augmented myogenic tone, which can be fully reversed in vitro by the competitive TNF α antagonist etanercept. TNF α mediates its effect via a sphingosine-1-phosphate (S1P)-dependent mechanism, requiring sphingosine kinase 1 and the S1P₂ receptor. In vivo, sphingosine kinase 1 deletion prevents and etanercept (2-week treatment initiated 6 weeks after myocardial infarction) reverses the reduction of cerebral blood flow, without improving cardiac function.

Conclusions—Cerebral artery vasoconstriction and decreased cerebral blood flow occur early in an animal model of heart failure; these perturbations are reversed by interrupting TNF α /S1P signaling. This signaling pathway may represent a potential therapeutic target to improve cognitive function in heart failure. (*Circulation*. 2012;126:196-206.)

Key Words: cerebrovascular circulation ■ myocardial infarction ■ signal transduction ■ sphingosine kinase ■ vasomotor system

This investigation sought to define the molecular mechanisms underlying reduced cerebral blood flow (CBF) in the early stages of heart failure (HF), when blood pressure remains minimally affected. Previous investigations have attempted to correlate reduced CBF in HF with deteriorating cardiac output (CO).¹⁻⁴ However, the correlation between CO and CBF is complex and depends on how cerebrovascular autoregulation adapts in HF. Under physiological conditions, autoregulation ensures that patients with adequate cerebro-

vascular reactivity can compensate for reduced CO by lowering cerebrovascular resistance (via dilation of brain arterioles).⁵ However, clinical data suggest that under conditions of HF, cerebrovascular resistance actually increases,^{3,4} although vasodilation should prevail. Enhanced vasoconstriction in HF may seriously compromise CBF autoregulation, creating the scenario in which further drops in CO may not be tolerated and the risk of developing structural and functional brain deficits may be increased.

Received October 7, 2010; accepted May 18, 2012.

From the Department of Physiology (J.Y., M.H.N.-A., A. Meissner, J.V.-B., J.T.K., A.K., S.P.H., H.Z., S.G.M., D.L., M.H., S.S.B.), Toronto Centre for Microvascular Medicine (J.V.-B., D.L., S.S.B.), Department of Medical Biophysics (M.v.E., R.M.H.), Heart and Stroke/Richard Lewar Centre of Excellence for Cardiovascular Research (S.P.H., M.H., S.S.B.), and Department of Medicine (M.H.), University of Toronto; Division of Cell and Molecular Biology, Toronto General Hospital Research Institute (M.H.N.-A., A. Momen, M.H.); Li Ka Shing Knowledge Institute (J.V.-B., D.L., S.S.B.) and Department of Anesthesia (J.V.-B.), St. Michael's Hospital; Department of Radiation Oncology, Princess Margaret Hospital (W.F., D.J.); and Mouse Imaging Centre, Toronto Centre for Phenogenomics (M.v.E., R.M.H.), Toronto, Canada.

*Drs Yang, Noyan-Ashraf, Meissner, Husain, and Bolz contributed equally to this article.

The online-only Data Supplement is available with this article at <http://circ.ahajournals.org/lookup/suppl/doi:10.1161/CIRCULATIONAHA.111.039644/-/DC1>.

Correspondence to Steffen-Sebastian Bolz, MD, PhD, Department of Physiology, Heart and Stroke/Richard Lewar Centre of Excellence in Cardiovascular Research, University of Toronto, Medical Science Bldg, Room 3326, 1 King's College Circle, Toronto, Ontario, M5S 1A8, Canada. E-mail sts.bolz@utoronto.ca

© 2012 American Heart Association, Inc.

Circulation is available at <http://circ.ahajournals.org>

DOI: 10.1161/CIRCULATIONAHA.111.039644

Clinical Perspective on p 206

Blood flow autoregulation relies on the property of cerebral arteries to adjust their flow resistance, via changes in vessel diameter, to the prevalent transmural pressure (ie, the myogenic response or Bayliss effect^{6,7}) and to maintain constant CBF over a wide range of systemic pressures (60- to 150-mm Hg mean arterial pressure).⁸ To ensure that CBF regulation has fine spatial resolution (ie, the ability to precisely and selectively increase flow to active brain volumes), different branch generations of the cerebrovascular tree are structurally and functionally specialized. The distal resistance arteries, which are located just before the capillary beds, exhibit the largest degree of myogenic activity and integrate modulatory influences of tissue-derived signaling molecules.⁹ Proximal cerebral arteries minimally restrict blood flow (ie, maintain a low-resistance profile) and ultimately display a functional pattern very similar to that of conduit arteries in the systemic circulation (ie, minimal myogenic activity). Therefore, high levels of myogenic tone in proximal cerebral arteries may result in widespread reductions in CBF.

With regard to the molecular basis for the myogenic response, sphingosine-1-phosphate (S1P) signaling has emerged as a central pathway in several vascular beds, including cerebral arteries.^{10–12} The procontractile effects of S1P are mediated primarily via the S1P₂ receptor,^{11–13} which activates RhoA/Rho kinase and ultimately inhibits myosin light-chain phosphatase.¹⁴ The central element of this pressure-sensitive signaling pathway in smooth muscle cells is sphingosine kinase 1 (Sphk1), which generates S1P. Thus, factors known to modulate Sphk1 activity are candidates for altering myogenic responsiveness.

The inflammatory cytokine tumor necrosis factor- α (TNF α) is a well-characterized activator of Sphk1^{15–17} and a hallmark of several cardiovascular^{18,19} and cerebrovascular^{20–22} diseases. Indeed, recent *in vitro* measurements using the spiral modiolar artery (a cochlear artery) indicate that TNF α activates smooth muscle cell Sphk1 to induce a procontractile state throughout the cochlear microcirculation.²³ In addition, TNF α has been shown to elicit vasoconstriction in both human mammary arteries²⁴ and mouse cerebral arteries.²⁵ However, the ability of TNF α to link a systemic disease like HF to altered control of CBF had not been explored.

Here, we show that proximal cerebral arteries, which normally possess minimal myogenic activity, are recruited to become myogenically active in HF and that TNF α is the primary factor driving this recruitment through activation of S1P signaling. Our results provide a microvascular concept that explains the association between HF and the decrease in CBF.

Methods

Mouse Nomenclature

All wild-type mice used in this investigation were commercially available C57BL/6N mice. Mice lacking Sphk1 (*Sphk1*^{-/-}), sphingosine kinase 2 (*Sphk2*^{-/-}), the S1P₂ receptor subtype (*S1P2R*^{-/-}), and a double mutant with complete deletion of Sphk1 and heterozygosity for Sphk2 (*Sphk1*^{-/-}/*Sphk2*[±]) were kindly provided by Dr Richard L. Proia (Bethesda, MD). Unless otherwise designated,

arteries were isolated from naïve mice; all mice operated on to induce HF or to create a sham controls were designated as such.

Myocardial Infarction

HF in mice was induced by experimental myocardial infarction produced by permanent surgical ligation of the left anterior descending coronary artery (LAD), as previously described.¹² In sham-operated controls, the thorax and pericardium were opened, but the LAD was not ligated. After either procedure, the chest was closed and the mice were extubated on spontaneous respiration. Cerebral arteries were isolated 4 to 6 weeks after myocardial infarction. As described, HF (infarct size approximating 25% of the left ventricular wall) mice develop enlarged hearts, congested lungs, reduced CO and blood pressure, and elevated peripheral resistance.¹² All of these parameters remain normal in sham-operated controls.

Isolation and Functional Assessment of Cerebral Arteries

To demonstrate the longitudinal gradient of myogenic activity, posterior cerebral artery (PCA) segments from healthy gerbils were used; distal segments of gerbil PCAs were more reliable for experimentation, because of less frequent branching. All other experiments used proximal PCA segments from the mouse. After anesthesia, the animal was decapitated, and the brain was rapidly removed from the cranium and immersed in ice-cold sterile 3-(*n*-morpholino)propanesulfonic acid (MOPS) buffer. PCA segments (0.8–1.0 mm in length) were carefully dissected from the surrounding connective tissue. Only first-order vessels were isolated from mice (160–220 μ m), whereas first- and third- or fourth-order vessels were harvested from gerbils (160–220 and 90–150 μ m in diameter, respectively). The isolated vessel segments were cannulated on glass micropipettes, stretched to their *in vivo* lengths, and pressurized to 45 mm Hg, as previously described.²⁶ All functional experiments were conducted in MOPS-buffered saline at 37°C with no perfusion.

To measure myogenic responses, vessels were subjected to stepwise increases in transmural pressure (20-mm Hg increments) from 20 to 100 mm Hg. At each pressure step, vessel diameter (dia_{active}) was measured once a steady state was reached (3–5 minutes). Myogenic tone was calculated as the percent constriction in relation to the maximal diameter at each respective transmural pressure: tone (percent of dia_{max}) = [(dia_{max} - dia_{active}) / dia_{max}] \times 100, where dia_{active} is the vessel diameter in MOPS containing Ca²⁺ and dia_{max} is the diameter in Ca²⁺-free MOPS. Vasomotor responses (eg, phenylephrine, acetylcholine, Ca²⁺ sensitivity) used the same calculation, only in these cases, dia_{active} represents the vessel diameter at steady state after application of the given agent and dia_{max} represents the maximal diameter (measured under Ca²⁺-free conditions) at 45 mm Hg. Further details are provided in the online-only Data Supplement, and representative tracings are shown in Figure I in the online-only Data Supplement.

Immunohistochemistry and Reverse Transcriptase–Polymerase Chain Reaction

Standard immunohistochemical and biochemical procedures were used. Detailed methods are provided in the online-only Data Supplement.

Cerebral Blood Flow

A noninvasive magnetic resonance imaging–based method known as the flow-sensitive alternating inversion recovery technique was used to evaluate brain perfusion.²⁷ This technique is described in detail in the online-only Data Supplement. Briefly, the approach isolates perfusion as an accelerated T1 signal relaxation. Magnetic resonance imaging signals were acquired from vertical sections of the forebrain, midbrain, and hindbrain, which correspond to the anterior, mixed, and posterior circulations. Flow-sensitive alternating inversion recovery images were evaluated for designated regions of interest by the use of standardized algorithms and image processing

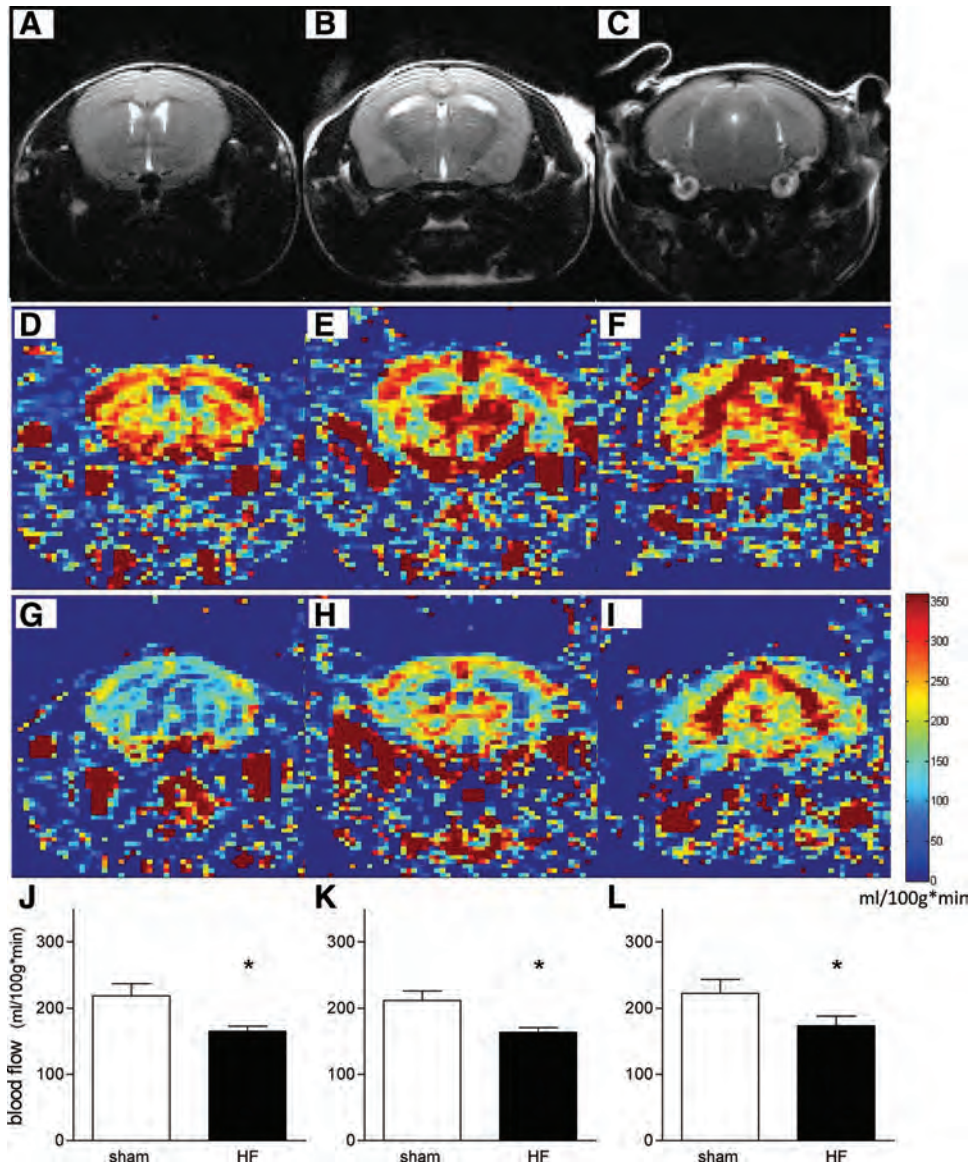


Figure 1. Heart failure (HF) reduces cerebral blood flow. Flow-sensitive alternating inversion recovery–magnetic resonance imaging of the forebrain (A), midbrain (B), and hindbrain (C) was used to assess blood flow in predefined cortical and subcortical brain regions of interest in sham (D–F) and HF (G–I) mice. HF significantly reduced global (J), cortical (K), and subcortical (L) blood flow compared with sham-treated mice (sham, $n=14$; HF, $n=16$). * $P<0.05$.

procedures (MIPAV; National Institutes of Health, Bethesda, MD; <http://www.mipav.cit.nih.gov>).

Etanercept Treatment In Vivo

Six weeks after myocardial infarction, cohorts of HF mice were treated with either etanercept (1 mg/mL sc) or saline twice weekly for 2 weeks. Sham-operated mice served as controls. CBF²⁷ and hemodynamic parameters¹² were assessed as previously described.

Statistical Analysis

All data (including figures) are expressed as mean \pm SEM, where n is the number of vessels studied. An unpaired Student t test was used to compare 2 separate groups (eg, sham and HF). When appropriate (eg, before and after inhibitor), a paired Student t test was used. For comparison of multiple groups, an ANOVA followed by t tests with Bonferroni correction was used. Differences were considered significant at $P<0.05$.

Results

Magnetic Resonance Imaging–Demonstrable Reductions in CBF Occur Early in HF

CBF was measured in predefined cortical and subcortical regions of interest, and pooling of data from all regions of interest was used to assess global CBF in sham ($n=14$) versus HF (4–6 weeks after myocardial infarction; $n=16$) mice. Global (227 ± 10 versus 165 ± 8 mL \cdot 100 g⁻¹ \cdot min⁻¹; $P<0.05$), cortical (213 ± 11 versus 163 ± 7 mL \cdot 100 g⁻¹ \cdot min⁻¹; $P<0.05$), and subcortical (226 ± 14 versus 185 ± 17 mL \cdot 100 g⁻¹ \cdot min⁻¹; $P<0.05$) CBF was reduced in HF mice (Figure 1). Importantly, these reductions in CBF were not attributable to any changes in brain structure, as measured by high-resolution magnetic resonance imaging (Figure II in the online-only Data Supplement). Moreover, at this early stage of HF, mice did not manifest

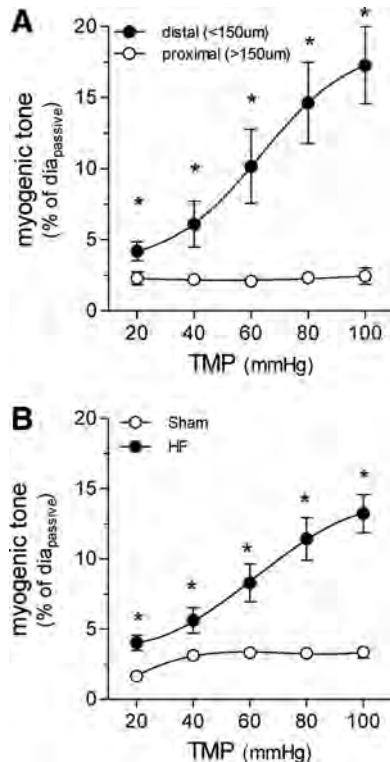


Figure 2. Heart failure (HF) enhances posterior cerebral artery (PCA) tone. **A**, Proximal (first order; passive external diameter at 45 mm Hg: $196 \pm 12 \mu\text{m}$) and distal (third or fourth order; passive external diameter at 45 mm Hg: $137 \pm 4 \mu\text{m}$) gerbil PCAs were subjected to stepwise increases in transmural pressure (TMP; 20–100 mm Hg). At each pressure step, myogenic tone was significantly larger in distal PCAs compared with proximal PCAs ($n=6$ for each group). **B**, Myogenic tone at every applied transmural pressure (20–100 mm Hg) was significantly enhanced in proximal PCAs isolated from mice with HF compared with sham-operated controls (sham, $n=6$; HF, $n=14$). * $P<0.05$.

cognitive abnormalities, as determined by the Morris water maze test (Figure III in the online-only Data Supplement).

HF Is Associated With Increased Myogenic Tone in Proximal Cerebral Arteries

In the gerbil, a larger animal enabling comparisons between proximal and distal cerebral vessels, we found that distal (third- or fourth-order) segments of the PCA normally exhibit greater resting tone (defined as tone at 45 mm Hg; distal, $7.1 \pm 2.7\%$; proximal, $1.9 \pm 0.2\%$; $n=6$; $P<0.05$) and significantly stronger myogenic tone at each applied pressure step (defined as tone over a range of 20–100 mm Hg in 20-mm Hg increments) compared with proximal (first-order) segments (Figure 2A).

In contrast, in mice with HF, both resting tone (sham, $3.0 \pm 0.3\%$, $n=6$; HF, $5.7 \pm 0.9\%$, $n=12$; $P<0.05$) and myogenic tone (Figure 2B) were significantly increased in proximal PCAs compared with sham-operated controls; passive external diameters did not differ (dia_{max} : sham, $197 \pm 2 \mu\text{m}$, $n=6$; HF, $195 \pm 3 \mu\text{m}$, $n=14$; $P=\text{NS}$).

Increased PCA Expression of TNF α Accounts for Enhanced Myogenic Tone in HF

Costaining of brain slices revealed increased TNF α expression in PCAs from mice with HF compared with sham

controls (Figure 3A). This increased TNF α expression appeared to be localized primarily to the smooth muscle compartment within the microvascular wall (virtually complete overlap of TNF α with smooth muscle α -actin staining; Figure 3B). Reverse transcriptase–polymerase chain reaction experiments using isolated PCAs confirmed a 2.5-fold increase in TNF α mRNA in HF versus sham (Figure 3C).

In PCAs isolated from wild-type mice with HF, etanercept (a competitive TNF α antagonist) fully normalized HF-stimulated enhancement of myogenic tone ($n=6$; Figure 3D). Consistent with this observation, treatment of PCAs isolated from naïve wild-type mice with TNF α (50 $\mu\text{g}/\text{mL}$ for 30 minutes) stimulated a significant increase in both resting tone ($2.4 \pm 0.1\%$ versus $4.5 \pm 0.5\%$; $n=5$; $P<0.05$, paired comparison) and myogenic tone (Figure 3E). Subsequent cotreatment with the putative S1P₂R antagonist JTE013 (1 $\mu\text{mol}/\text{L}$ for 30 minutes) abolished the TNF α -mediated increase in resting tone ($2.7 \pm 0.4\%$; $P=\text{NS}$, paired comparison with control) and myogenic tone (Figure 3E).

TNF α Increases Myogenic Tone in Mouse PCA via Sphk1 and S1P₂R

On the basis of our observation that an S1P₂R antagonist abolished TNF α -enhanced tone in PCAs from wild-type animals without HF, we hypothesized that the increased myogenic tone of PCAs from mice with HF might also be mediated by enhanced S1P/S1P₂R signaling via the known TNF α -dependent activation of the enzyme sphingosine kinase (*Sphk*).^{15–17,23} First, we confirmed that a low concentration of S1P (10 nmol/L, which does not stimulate vasoconstriction) has the ability to enhance resting and myogenic tone in wild-type mouse and gerbil PCAs (Table I in the online-only Data Supplement). Next, using loss-of-function mice (please note that the *Sphk1*^{-/-}/*Sphk2*^{-/-} double knockout is embryonically lethal), we observed that TNF α had no effect on PCAs from *Sphk1*^{-/-}, *Sphk1*^{-/-}/*Sphk2*^{+/-}, or *S1P₂R*^{-/-} mice (Figure 4). In contrast, TNF α stimulated a 2- to 3-fold increase in myogenic tone in mice lacking *Sphk2* (Figure 4A).

Enhanced Myogenic Tone in the PCA in HF Is Mediated by Activation of S1P Signaling

Unlike wild-type mice (Figure 2B), HF failed to augment myogenic tone in mice lacking *Sphk1* (Figure 5A). Importantly, the application of exogenous S1P (3 $\mu\text{mol}/\text{L}$) restored the HF phenotype and enhanced myogenic tone in PCAs isolated from both HF and sham *Sphk1*^{-/-} mice to similar extents (Figure 5A). Passive external diameters were not different (dia_{max} : *Sphk1*^{-/-} sham, $174 \pm 7 \mu\text{m}$, $n=6$; *Sphk1*^{-/-} HF, $173 \pm 8 \mu\text{m}$, $n=5$; $P=\text{NS}$; Figure 5A). Our model of HF also failed to increase myogenic tone in mice lacking the S1P₂ receptor (*S1P₂R*^{-/-}; Figure 5B). Again, passive diameters did not differ (dia_{max} : *S1P₂R*^{-/-} sham, $186 \pm 13 \mu\text{m}$, $n=5$; *S1P₂R*^{-/-} HF, $191 \pm 4 \mu\text{m}$, $n=6$; $P=\text{NS}$; Figure 5B). As with the TNF α -mediated enhancement of myogenic tone (Figure 3E), JTE013 reversed the HF-stimulated enhancement of myogenic tone observed in PCAs from wild-type mice (Figure 5C).

Taken together, these data demonstrate that the enhanced myogenic tone of PCAs that occurs in HF requires an intact S1P signaling system. To further establish the specificity of

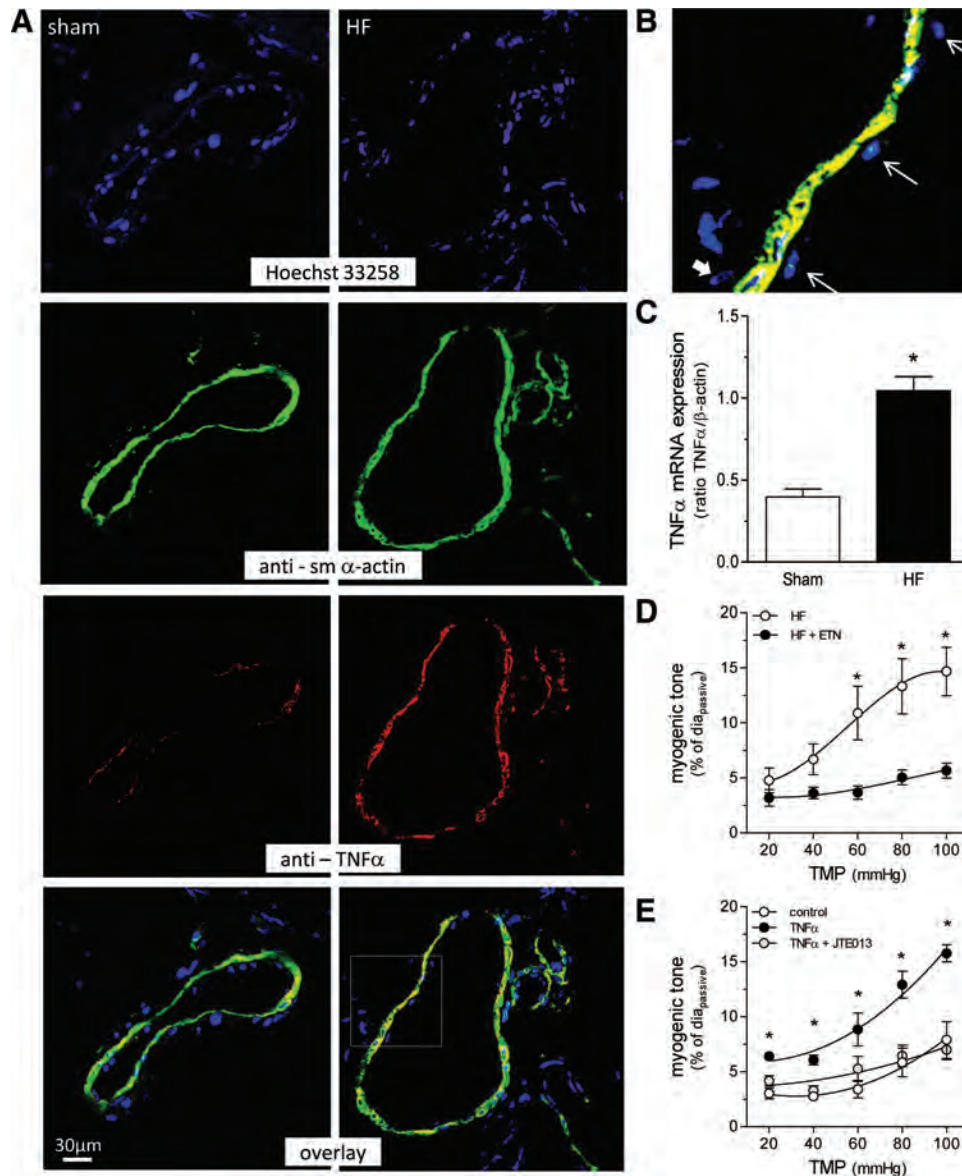


Figure 3. Tumor necrosis factor- α (TNF α) mediates the heart failure (HF)-induced increase in posterior cerebral artery (PCA) myogenic tone. **A**, Brain slices from HF and sham-operated animals containing a cross section of the PCA were costained with Hoechst 33258 (to identify cell nuclei) and antibodies against smooth muscle α -actin (sm α -actin) and TNF α . TNF α expression was increased homogeneously throughout the PCA vessel wall in HF mice (overlay). **B**, High-magnification confocal images demonstrate that the vast majority of TNF α expression was localized to the smooth muscle layer (colocalization of sm α -actin and TNF α generates yellow); TNF α expression was not observed in the endothelial (thin arrows identify endothelial nuclei) or adventitial (thick arrow identifies adventitial nuclei) layers. **C**, TNF α mRNA expression was higher in isolated PCAs from HF mice compared with sham-operated animals ($n=4$, each). **D**, The TNF α antagonist etanercept (ETN; 10 μ g/mL for 30 minutes; $dia_{max}=194\pm 3$ μ m; $n=6$) normalized the HF-mediated increase in myogenic tone. **E**, TNF α (50 pg/mL for 30 minutes) stimulated a significant enhancement of myogenic tone in wild-type PCAs that was reversed by subsequent treatment with JTE013 (1 μ mol/L for 30 minutes; $n=5$). TMP indicates transmural pressure.

our earlier observations with the TNF α antagonist etanercept (Figure 3D), we tested the effects of this agent in mice lacking components of S1P signaling. Etanercept had no effect on PCAs isolated from *Sphk1*^{-/-} or *Sphk1*^{-/-}/*Sphk2*^{+/-} mice with HF (Figure IV in the online-only Data Supplement). Although a small effect of etanercept was observed in PCAs from *SIP2R*^{-/-} mice with HF (Figure V in the online-only Data Supplement), it was not enough to account for the complete normalization of myogenic tone observed in PCAs from wild-type mice with HF (Figure 3D).

HF Specifically Enhances S1P-Stimulated PCA Vasoconstriction

We next examined whether HF was associated with indiscriminate (ie, systematic) increases in PCA responsiveness or a more exclusive sensitivity to S1P. PCAs from sham mice displayed minimal vasoconstriction in response to exogenously applied S1P (30 nmol/L to 3 μ mol/L; Figure 6A), whereas PCAs from HF mice displayed robust dose-dependent vasoconstrictor responses to S1P (Figure 6A). In contrast, dose-response relationships for phenylephrine (\log_{EC50} : HF, -5.33 ± 0.34 ; sham,

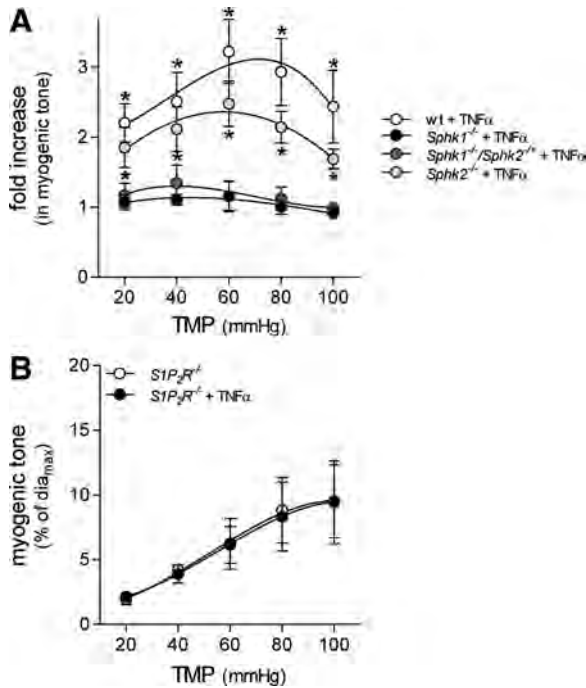


Figure 4. Tumor necrosis factor- α (TNF α) requires sphingosine kinase 1 (Sphk1) to increase myogenic tone in posterior cerebral arteries (PCAs). **A**, TNF α failed to enhance myogenic tone in PCAs isolated from *Sphk1*^{-/-} (dia_{max}=167 \pm 4 μ m; n=11) or *Sphk1*^{-/-}/*Sphk2*^{+/-} mice (dia_{max}=181 \pm 4 μ m; n=6). Mice lacking Sphk2 (*Sphk2*^{-/-}, n=5) showed TNF α -induced increases in myogenic tone that were not different from those observed in wild-type (wt) mice (n=8). Data are normalized to the untreated control level of myogenic tone. **B**, PCAs isolated from *S1P₂R*^{-/-} mice showed no increase in myogenic tone after TNF α treatment (50 pg/mL for 30 minutes; dia_{max}=188 \pm 12 μ m; n=4). **P*<0.05 for unpaired (**A**) and paired (**B**) comparisons. TMP indicates transmural pressure.

-5.33 \pm 0.27; *P*=NS; n=4 each; Figure 6B) and Ca²⁺ under depolarizing (120 mmol/L K⁺) conditions (log_{EC50}: HF, -3.28 \pm 0.05; sham, -3.31 \pm 0.05; *P*=NS; n=4 each; Figure 6C) were not affected by HF.

Lack of *Sphk1*^{-/-} Protects Against the HF-Induced Reduction in CBF

Our in vitro data predict that disrupting S1P signaling will ameliorate the HF-induced reduction in CBF. LAD ligation profoundly compromised cardiac performance in *Sphk1*^{-/-} mice, as evidenced by substantial reductions in stroke volume and CO (Table II in the online-only Data Supplement). A compensatory increase in total peripheral resistance maintained mean arterial pressure (MAP) in *Sphk1*^{-/-} mice, with HF at levels comparable to those in sham-operated mice (Table II in the online-only Data Supplement). Although MAP levels appeared to be lower than in the other tested cohorts, these observations are unlikely to be attributable to the *Sphk1*^{-/-} genotype.²⁸

Because autoregulation serves to maintain organ blood flow during fluctuations in perfusion pressure, the observed lack of correlation between CBF and MAP in *Sphk1*^{-/-} sham and HF mice indicates that autoregulatory mechanisms were functioning under both conditions (Figure 7). Despite intact autoregulation, CBF measures were qualitatively lower than

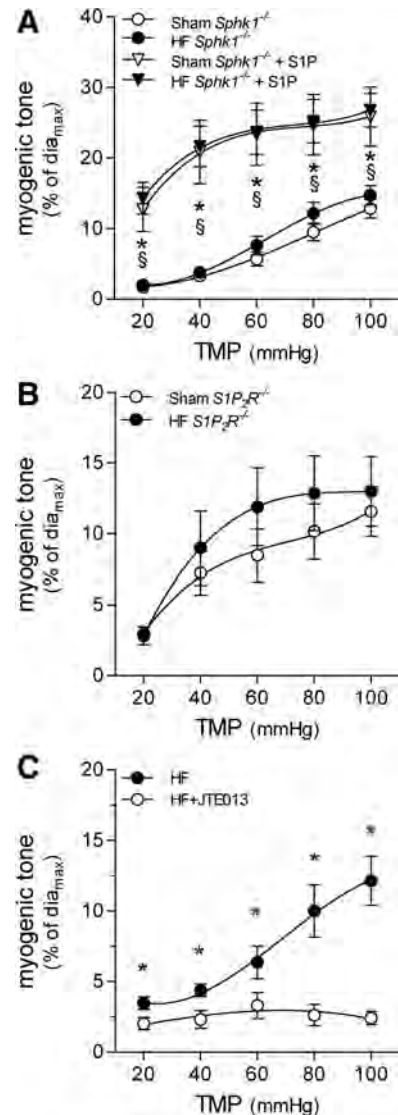


Figure 5. Increases in myogenic tone in heart failure (HF) require Sphk1 and the sphingosine-1-phosphate-2 receptor (S1P₂R). **A**, Myogenic tone in posterior cerebral arteries (PCAs) isolated from Sphk1 knockout mice with HF (*Sphk1*^{-/-} HF; n=5) did not differ from corresponding sham control (*Sphk1*^{-/-} sham; n=6; *P*=NS, unpaired comparison). Exogenous S1P (3 μ mol/L) enhanced myogenic tone in both groups to a similar extent (*P*=NS, unpaired comparison). **P*<0.05 for paired comparisons of *Sphk1*^{-/-} sham vs *Sphk1*^{-/-} sham+S1P; §*P*<0.05 for paired comparisons of *Sphk1*^{-/-} HF vs *Sphk1*^{-/-} HF+S1P. **B**, Myogenic tone in PCAs isolated from *S1P₂R* knockout mice with HF (*S1P₂R*^{-/-} HF; n=6) also did not differ (*P*=NS, unpaired comparison) from corresponding sham control (*S1P₂R*^{-/-} sham; n=5). **C**, JTE013 (1 μ mol/L for 30 minutes) reversed the enhancement of myogenic tone observed in PCAs isolated from wild-type mice with HF (n=8). **P*<0.05 for paired comparisons. TMP indicates transmural pressure.

in the other cohorts, suggesting the presence of a specific *Sphk1*^{-/-} phenotype. Our experimental design, however, did not include wild-type littermate controls; thus, we limit our analyses strictly to the sham and HF groups within the *Sphk1*^{-/-} cohort. In this specific context, HF did not alter CBF in *Sphk1*^{-/-} mice (Figure 7C), so we conclude that *Sphk1* is an integral component of the signaling pathway that reduces CBF in HF.

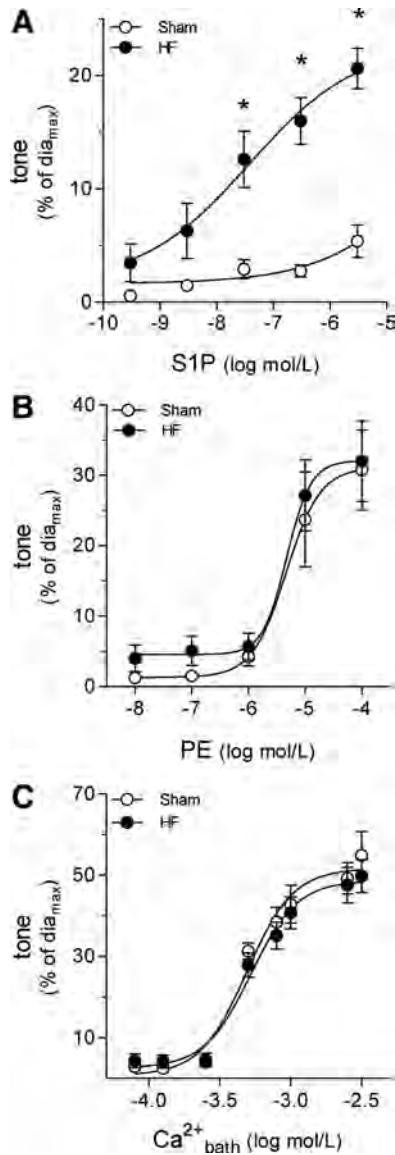


Figure 6. Heart failure (HF) selectively enhances sphingosine-1-phosphate (S1P)-induced constriction of posterior cerebral arteries (PCAs). **A**, S1P-stimulated vasoconstriction in PCAs isolated from mice with HF was significantly enhanced in mice with HF compared with sham controls (sham, $n=4$; HF, $n=9$). In contrast, dose-response relationships for **(B)** phenylephrine (PE; both groups, $n=4$) and **(C)** Ca^{2+} under depolarizing conditions (both groups, $n=4$) were unaffected by HF. All vasomotor response data were obtained at a transmural pressure of 45 mm Hg. * $P<0.05$ for unpaired comparisons; § $P<0.05$ for paired comparisons of HF vs HF+JTE013.

Systemic Etanercept Treatment of Mice in HF Improves Global CBF

We next attempted to therapeutically target the identified molecular pathway driving reduced CBF. In the absence of a clinically available S1P signaling antagonist, we used etanercept, a clinically available TNF α antagonist.

In initial experiments, the etanercept treatment was started 2 weeks after LAD ligation (1 mg/mL sc twice per week for 6 weeks). Etanercept treatment fully reversed the reduction in global CBF observed in HF (sham saline, $220\pm 8 \text{ mL} \cdot 100 \text{ g}^{-1} \cdot \text{min}^{-1}$, $n=8$; HF saline: $189\pm 7 \text{ mL}/100 \text{ g} \cdot \text{min}$, $n=8$;

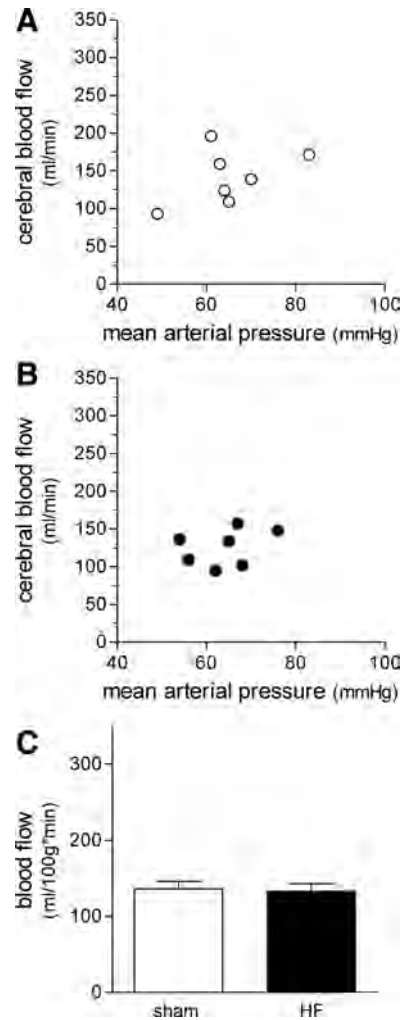


Figure 7. Heart failure (HF) does not alter cerebral blood flow or autoregulation in $\text{Sphk1}^{-/-}$ mice. No correlation between mean arterial pressure and cerebral blood flow (CBF) was evident in **(A)** sham-operated $\text{Sphk1}^{-/-}$ mice and **(B)** $\text{Sphk1}^{-/-}$ mice with HF, indicating the presence of blood flow autoregulation. **C**, Global CBF was unaffected by HF in $\text{Sphk1}^{-/-}$ mice. For both groups, $n=8$.

HF+etanercept, $228\pm 5 \text{ mL} \cdot 100 \text{ g}^{-1} \cdot \text{min}^{-1}$, $n=7$; $P<0.05$, HF versus sham or HF+etanercept; Table III in the online-only Data Supplement). However, this regimen also positively affected cardiac function (Table III in the online-only Data Supplement), making it difficult to attribute the positive outcome unambiguously to a vascular mechanism.

In subsequent experiments, etanercept treatment was initiated 6 weeks after LAD ligation (1 mg/mL sc twice per week for 2 weeks), under the premise that the heart injury would be more permanent at later time points following myocardial infarction. Indeed, this revised treatment regimen did not improve cardiac function (eg, CO, LVEF, stroke volume; Table IV in the online-only Data Supplement) but continued to restore CBF (Figure 8; representative flow-sensitive alternating inversion recovery-magnetic resonance imaging flow maps are displayed in Figure VI in the online-only Data Supplement).

Although both CO (inversely) and total peripheral resistance (positively) showed tight correlation with infarct size, MAP did not (Figure 8). Similarly, CBF was inversely

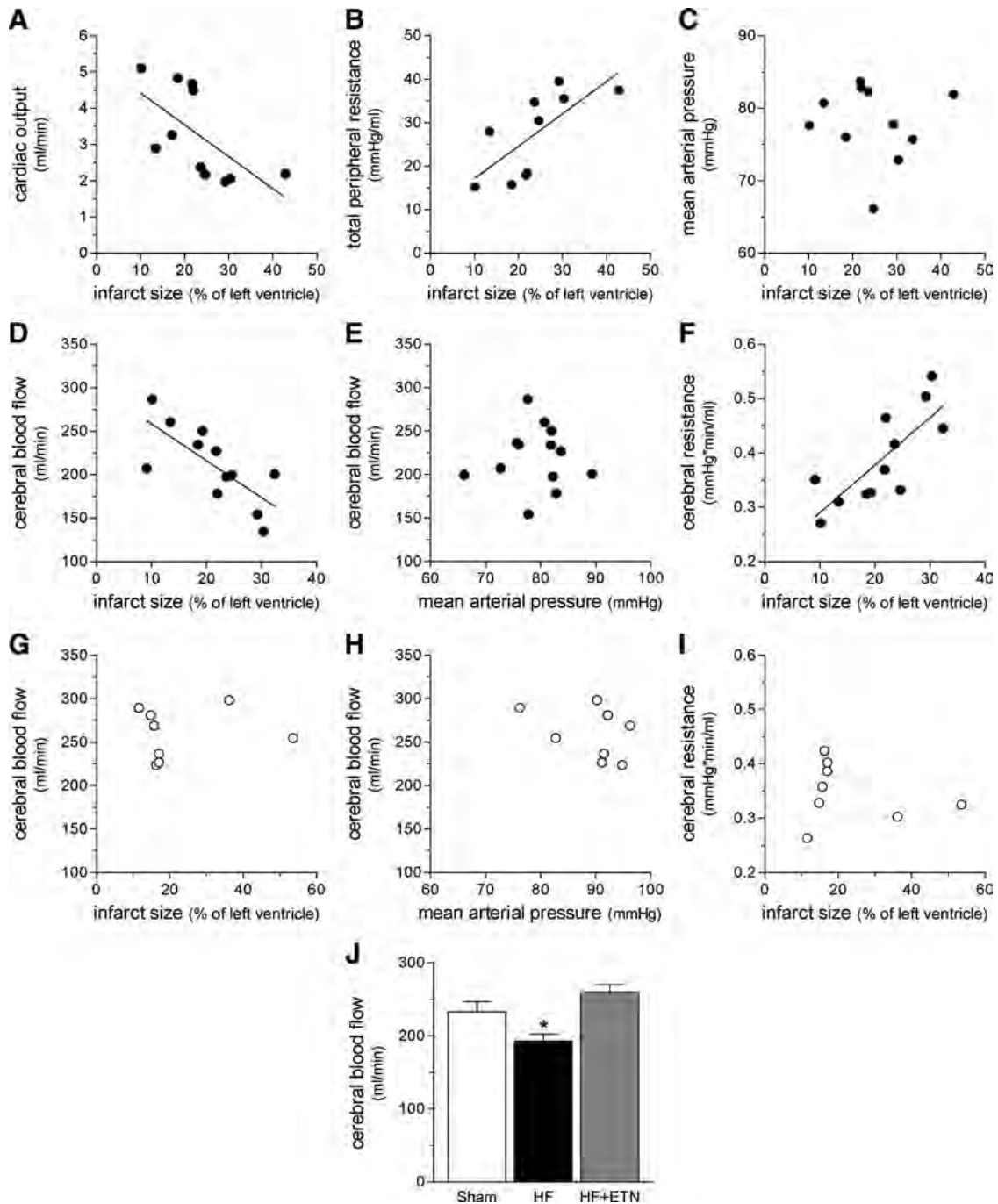


Figure 8. Correlation of systemic and cerebral hemodynamic parameters to infarct size. In heart failure (HF) mice (n=12), (A) cardiac output correlates inversely, (B) total peripheral resistance correlates positively, and (C) mean arterial pressure (MAP) does not correlate with infarct size. D, Cerebral blood flow (CBF) correlates inversely with infarct size but (E) does not correlate with MAP; instead, (F) the calculated values for cerebral resistance (MAP/CBF) positively correlate with infarct size. In contrast to saline-treated HF mice, (G) CBF does not correlate with infarct size in etanercept (ETN)-treated mice (initiated 6 weeks after left anterior descending ligation; n=8). Additionally, no correlations between (H) CBF and MAP or (I) cerebral resistance and infarct size are observed. J, Pooled data show that CBF in mice with HF (n=30) is $\approx 20\%$ lower than in sham-operated controls (n=28); etanercept treatment normalizes CBF during heart failure (n=8). * $P < 0.05$ vs all other groups.

correlated with infarct size but not MAP; instead, CBF was negatively correlated with calculated values for cerebral resistance (MAP/CBF). In contrast, etanercept-treated mice (6 weeks after LAD ligation; n=8) displayed no correlations between CBF and infarct size, CBF, and MAP or between cerebral resistance and infarct size.

Discussion

This investigation demonstrates that HF induces a widespread peripheral vascular response that includes an alteration in CBF autoregulation. In response to reduced CO, total peripheral resistance increases,^{29,30} which maintains MAP well within the acceptable range for blood flow autoregulation (ie,

60–150 mm Hg).⁸ This compensatory mechanism explains why MAP does not correlate with infarct size (Figure 8C).

Because MAP is maintained within the autoregulatory range, the observed reductions in CBF cannot be attributed to systemic hemodynamic parameters. The absence of a relationship between MAP and CBF in HF (Figure 8E) demonstrates that CBF autoregulation persists under these conditions, with reductions in CBF resulting from altered autoregulatory mechanisms within the cerebral microcirculation (ie, increased resistance at a given MAP). Together, these data suggest that HF induces a compensatory vascular response that serves to maintain MAP by elevating total peripheral resistance. CBF autoregulation is not exempted from this response. Indeed, the degree to which cerebral resistance increases is tightly correlated with the degree of heart injury (ie, infarct size; Figure 8F).

The reduction in CBF observed in this investigation is consistent with clinical reports in HF patients.^{1–4} Reduced perfusion of the brain would be expected to cause wide-ranging neurological effects; indeed, cognitive symptoms, including impairment of memory, attention, mental flexibility, and global cognitive functions, are clinically observed in 40% to 60% of patients with late-stage HF.^{1,2,31,32} The 25% CBF reduction observed in the present investigation, however, is below the reported threshold^{33–36} necessary to cause cognitive deficits or gross morphological changes and explains their absence in the present model.

In vitro, we confirm that a longitudinal gradient of myogenic activity exists within the cerebrovascular tree; proximal arteries display minimal myogenic tone, whereas the more distal sections possess substantial myogenic activity. Our results support the premise that proximal PCA branches do not play a primary role in adjusting CBF under normal physiological conditions. In HF, their phenotype changes: they display augmented myogenic tone that, under physiological conditions, is more characteristic of distal regions. In essence, myogenic reactivity and consequently microvascular resistance to blood flow extends to the proximal regions of the vascular tree, resulting in reduced cerebral blood supply.

The recruitment of PCAs into the myogenic chain results from an autocrine/paracrine effect of TNF α , which is released from PCA vascular wall. Although TNF α has a well-documented role in stroke³⁷ and HF,^{18,19} further studies are required to determine how HF actually activates TNF α in the PCA. Of note, we recently implicated TNF α -dependent signaling in the cochlear microcirculation as a pathogenic stimulus in sensorineuronal hearing loss.²³ The vascular effects of TNF α are generally attributed to increased serum levels of the cytokine; however, the present study demonstrates that HF induces an upregulation of TNF α mRNA and protein expression within the vascular wall of PCAs, with the vast majority of protein localized to the smooth muscle layer. We therefore propose that TNF α (or more specifically, the relevant pool of smooth muscle cell TNF α) acts in an autocrine/paracrine manner to enhance PCA smooth muscle cell contractility. This would explain why explanted PCAs retain their altered phenotype, characterized by augmented myogenic tone, over several hours ex vivo. Sequestering vessel wall TNF α with etanercept restores tone in HF PCAs

to sham levels, confirming that TNF α is causally involved in the tone-enhancing mechanism and that the vessel wall is the source of TNF α . Accordingly, exogenously applied TNF α induces the same phenotype shift in isolated proximal PCAs from naïve mice that was observed in HF mice (ie, from minimal to robust myogenic tone).

The molecular pathway that links TNF α to enhanced myogenic tone is the S1P signaling pathway. Consistent with our previous observations,¹⁴ S1P signaling is a key regulator of myogenic tone^{11–13} and is essential for the HF-mediated increase in proximal PCA myogenic tone. Using knockout models, we show that exogenous TNF α , a known activator of *Sphk1*,^{15–17} mediates its effects via *Sphk1* and *SIP₂R*. Specifically, isolated PCAs from mice lacking *Sphk1* (*Sphk1*^{-/-}), *Sphk1*, and 1 allele of *Sphk2* (*Sphk1*^{-/-}/*Sphk2*[±]) or *SIP₂R* (*SIP₂R*^{-/-}) do not have increased myogenic tone in response to TNF α .

The deletion of *Sphk1* abolishes the HF-induced augmentation of PCA myogenic tone (measured in vitro) and protects against HF-mediated reductions in CBF and changes in CBF autoregulation. Genetic deletion of *SIP₂R* also abolished the HF-induced augmentation of myogenic tone in isolated PCAs. JTE013 reverses both the TNF α - and HF-mediated increase in myogenic tone. Although JTE013 is a putative *SIP₂R* antagonist, we observed clear *SIP₂R*-independent effects (Figure VII in the online-only Data Supplement).³⁸ Nevertheless, JTE013 appears to retain specificity for S1P signaling (ie, does not inhibit endothelin-1 or phenylephrine responses),^{12,23} making it suitable for investigating the contributions of S1P receptors, despite an inability to discern the specific role of *SIP₂R*. Taken together, our data support that TNF α mediates its effects via S1P signaling, a conclusion that is further substantiated by our observation that TNF α sequestration (etanercept) is without effect in isolated PCAs with disrupted S1P signaling.

To therapeutically translate our in vitro data, we targeted TNF α in vivo with the clinically available agent etanercept. By delaying treatment to 6 weeks after LAD ligation, we mitigated the beneficial effects of etanercept on cardiac function (compare Tables II and III in the online-only Data Supplement). In the absence of improved cardiac function, we are able to unambiguously attribute the restored CBF to altered vascular function. We found that etanercept treatment broke the link between heart injury and cerebrovascular resistance/CBF (ie, eliminated the correlations observed in saline-treated HF mice; Figure 8). Importantly, we continued to observe no correlation between MAP and CBF in etanercept-treated mice with HF, indicating the normalization of autoregulation.

Significantly, although etanercept improved CBF autoregulation, it did not meaningfully alter total peripheral resistance (Table IV). This suggests that etanercept treatment acts selectively on certain microvascular beds during HF and positions the treatment as a possible strategy to discretely improve blood flow in critical organs (eg, the brain) during HF. Critical organ perfusion was not assessed in the Randomized Etanercept North American Strategy to Study Antagonism of Cytokines (RENAISSANCE) and Research Into Etanercept Cytokine Antagonism in Ventricular Dysfunction

(RECOVER) clinical trials, which were halted prematurely owing to a lack of beneficial effects on the end points of clinical composite score, HF hospitalization, and mortality.³⁹ Importantly, these trials also showed that etanercept did not worsen the clinical outcome of HF.³⁹ This finding encourages a reexamination of this pathway for the improvement or prevention of cerebral perfusion deficits in HF.

Conclusions

We demonstrate that TNF α recruits proximal cerebral arteries into a myogenic phenotype, resulting in comprised autoregulation and restricted CBF. We demonstrate that TNF α mediates the enhancement of PCA tone via Sphk1/S1P₂R signaling, all of which deserve evaluation as potential therapeutic targets for the improvement of CBF in HF patients. Indeed, our data show that the *in vivo* use of etanercept fully restores CBF in mice with HF. We propose that etanercept treatment restores the minimally restrictive phenotype of PCAs and shifts autoregulatory function back to the distal regions of the cerebral microcirculation.

Sources of Funding

We gratefully acknowledge the operating, infrastructure, and salary funding support from the Canadian Institutes of Health Research (Dr Bolz, FRN-84402 and FRN-119345; Dr Husain, FRN-117801), Canadian Foundation for Innovation (Dr Bolz, 11810), Ontario Research Fund (Dr Bolz, RI#11810; Dr Henkelman, RE#03-051, and RE#02-002), Canadian Stroke Network (Dr Bolz), Heart and Stroke Foundation of Ontario New Investigator Award (Dr Bolz, NI6581) and Career Investigator Award (Dr Husain, CI5503), and Canada Research Chair in Imaging Technologies in Human Disease and Preclinical Models (Dr Henkelman, 950-203746), as well as startup funding from the University of Toronto (Dr Bolz).

Disclosures

None.

References

- Pressler SJ. Cognitive functioning and chronic heart failure: a review of the literature (2002-July 2007). *J Cardiovasc Nurs*. 2008;23:239–249.
- Vogels RL, Scheltens P, Schroeder-Tanka JM, Weinstein HC. Cognitive impairment in heart failure: a systematic review of the literature. *Eur J Heart Fail*. 2007;9:440–449.
- Choi BR, Kim JS, Yang YJ, Park KM, Lee CW, Kim YH, Hong MK, Song JK, Park SW, Park SJ, Kim JJ. Factors associated with decreased cerebral blood flow in congestive heart failure secondary to idiopathic dilated cardiomyopathy. *Am J Cardiol*. 2006;97:1365–1369.
- Vogels RL, Oosterman JM, Laman DM, Gouw AA, Schroeder-Tanka JM, Scheltens P, van der Flier WM, Weinstein HC. Transcranial Doppler blood flow assessment in patients with mild heart failure: correlates with neuroimaging and cognitive performance. *Congest Heart Fail*. 2008;14:61–65.
- Georgiadis D, Sievert M, Cencetti S, Uhlmann F, Krivokuca M, Zierz S, Werdan K. Cerebrovascular reactivity is impaired in patients with cardiac failure. *Eur Heart J*. 2000;21:407–413.
- Hill MA, Zou H, Potocnik SJ, Meininger GA, Davis MJ. Invited review: arteriolar smooth muscle mechanotransduction: Ca(2+) signaling pathways underlying myogenic reactivity. *J Appl Physiol*. 2001;91:973–983.
- Schubert R, Lidington D, Bolz SS. The emerging role of Ca²⁺ sensitivity regulation in promoting myogenic vasoconstriction. *Cardiovasc Res*. 2008;77:8–18.
- Paulson OB, Strandgaard S, Edvinsson L. Cerebral autoregulation. *Cerebrovasc Brain Metab Rev*. 1990;2:161–192.
- Brekke JF, Gokina NI, Osol G. Vascular smooth muscle cell stress as a determinant of cerebral artery myogenic tone. *Am J Physiol Heart Circ Physiol*. 2002;283:H2210–H2216.
- Scherer EQ, Lidington D, Oestreicher E, Arnold W, Pohl U, Bolz SS. Sphingosine-1-phosphate modulates spiral modiolar artery tone: a potential role in vascular-based inner ear pathologies? *Cardiovasc Res*. 2006;70:79–87.
- Peter BF, Lidington D, Harada A, Bolz HJ, Vogel L, Heximer S, Spiegel S, Pohl U, Bolz SS. Role of sphingosine-1-phosphate phosphohydrolase 1 in the regulation of resistance artery tone. *Circ Res*. 2008;103:315–324.
- Hoefler J, Azam MA, Kroetsch JT, Poi HL, Momen MA, Voigtlaender-Bolz J, Scherer EQ, Meissner A, Bolz SS, Husain M. Sphingosine-1-phosphate-dependent activation of p38 MAPK maintains elevated peripheral resistance in heart failure through increased myogenic vasoconstriction. *Circ Res*. 2010;107:923–933.
- Lorenz JN, Arend LJ, Robitz R, Paul RJ, MacLennan AJ. Vascular dysfunction in S1P2 sphingosine 1-phosphate receptor knockout mice. *Am J Physiol Regul Integr Comp Physiol*. 2007;292:R440–R446.
- Bolz SS, Vogel L, Sollinger D, Derwand R, Boer C, Pitson SM, Spiegel S, Pohl U. Sphingosine kinase modulates microvascular tone and myogenic responses through activation of RhoA/Rho kinase. *Circulation*. 2003;108:342–347.
- Xia P, Wang L, Gamble JR, Vadas MA. Activation of sphingosine kinase by tumor necrosis factor-alpha inhibits apoptosis in human endothelial cells. *J Biol Chem*. 1999;274:34499–34505.
- Xia P, Gamble JR, Rye KA, Wang L, Hii CS, Cockerill P, Khew-Goodall Y, Bert AG, Barter PJ, Vadas MA. Tumor necrosis factor-alpha induces adhesion molecule expression through the sphingosine kinase pathway. *Proc Natl Acad Sci U S A*. 1998;95:14196–14201.
- Pitson SM, Moretti PA, Zebol JR, Lynn HE, Xia P, Vadas MA, Wattenberg BW. Activation of sphingosine kinase 1 by ERK1/2-mediated phosphorylation. *EMBO J*. 2003;22:5491–5500.
- El Sherif WT, El Tooney LF, Meki AR, Abdel Moneim A. Proinflammatory cytokines, soluble Fas receptor, nitric oxide and angiotensin converting enzyme in congestive heart failure. *Egypt J Immunol*. 2005;12:39–48.
- Pan JP, Liu TY, Chiang SC, Lin YK, Chou CY, Chan WL, Lai ST. The value of plasma levels of tumor necrosis factor-alpha and interleukin-6 in predicting the severity and prognosis in patients with congestive heart failure. *J Chin Med Assoc*. 2004;67:222–228.
- Sairanen T, Carpen O, Karjalainen-Lindsberg ML, Paetau A, Turpeinen U, Kaste M, Lindsberg PJ. Evolution of cerebral tumor necrosis factor-alpha production during human ischemic stroke. *Stroke*. 2001;32:1750–1758.
- Sairanen TR, Lindsberg PJ, Brenner M, Carpen O, Siren A. Differential cellular expression of tumor necrosis factor-alpha and type I tumor necrosis factor receptor after transient global forebrain ischemia. *J Neurol Sci*. 2001;186:87–99.
- Liu T, Clark RK, McDonnell PC, Young PR, White RF, Barone FC, Feuerstein GZ. Tumor necrosis factor-alpha expression in ischemic neurons. *Stroke*. 1994;25:1481–1488.
- Scherer EQ, Yang J, Canis M, Reimann K, Ivanov K, Diehl CD, Backx PH, Wier WG, Strieth S, Wangemann P, Voigtlaender-Bolz J, Lidington D, Bolz SS. TNF α enhances microvascular tone and reduces blood flow in the cochlea via enhanced S1P signaling. *Stroke*. 2010;41:2618–2624.
- Iversen PO, Nicolaysen A, Kvernebo K, Benestad HB, Nicolaysen G. Human cytokines modulate arterial vascular tone via endothelial receptors. *Pflugers Arch*. 1999;439:93–100.
- Vecchione C, Frati A, Di Pardo A, Cifelli G, Carnevale D, Gentile MT, Carangi R, Landolfi A, Carullo P, Bettarini U, Antenucci G, Mascio G, Busceti CL, Notte A, Maffei A, Cantore GP, Lembo G. Tumor necrosis factor-alpha mediates hemolysis-induced vasoconstriction and the cerebral vasospasm evoked by subarachnoid hemorrhage. *Hypertension*. 2009;54:150–156.
- Bolz SS, de Wit C, Pohl U. Endothelium-derived hyperpolarizing factor but not NO reduces smooth muscle Ca²⁺ during acetylcholine-induced dilation of microvessels. *Br J Pharmacol*. 1999;128:124–134.
- Kim SG. Quantification of relative cerebral blood flow change by flow-sensitive alternating inversion recovery (FAIR) technique: application to functional mapping. *Magn Reson Med*. 1995;34:293–301.
- Olivera A, Eisner C, Kitamura Y, Dillahun S, Allende L, Tuymetova G, Watford W, Meylan F, Diesner SC, Li L, Schnerrmann J, Proia RL, Rivera J. Sphingosine kinase 1 and sphingosine-1-phosphate receptor 2 are vital to recovery from anaphylactic shock in mice. *J Clin Invest*. 2010;120:1429–1440.
- Schrier RW, Abraham WT. Hormones and hemodynamics in heart failure. *N Engl J Med*. 1999;341:577–585.
- Halenda SP, Banga HS, Zavoico GB, Lau LF, Feinstein MB. Synergistic release of arachidonic acid from platelets by activators of protein

- kinase-C and Ca^{2+} ionophores: evidence for the role of protein phosphorylation in the activation of phospholipase-A2 and independence from the Na^+/H^+ exchanger. *Biochemistry*. 1989;28:7356–7363.
31. Almeida OP, Tamai S. Congestive heart failure and cognitive functioning amongst older adults. *Arq Neuropsiquiatr*. 2001;59:324–329.
 32. Sauve MJ, Lewis WR, Blankenbiller M, Rickabaugh B, Pressler SJ. Cognitive impairments in chronic heart failure: a case controlled study. *J Card Fail*. 2009;15:1–10.
 33. Baron JC. Perfusion thresholds in human cerebral ischemia: historical perspective and therapeutic implications. *Cerebrovasc Dis*. 2001;11(suppl 1):2–8.
 34. Marchal G, Beaudouin V, Rioux P, de la Sayette V, Le Doze F, Viader F, Derlon JM, Baron JC. Prolonged persistence of substantial volumes of potentially viable brain tissue after stroke: a correlative PET-CT study with voxel-based data analysis. *Stroke*. 1996;27:599–606.
 35. Marchal G, Benali K, Iglesias S, Viader F, Derlon JM, Baron JC. Voxel-based mapping of irreversible ischaemic damage with PET in acute stroke. *Brain*. 1999;122:2387–2400.
 36. Heiss WD, Grond M, Thiel A, von Stockhausen HM, Rudolf J, Ghaemi M, Lottgen J, Stenzel C, Pawlik G. Tissue at risk of infarction rescued by early reperfusion: a positron emission tomography study in systemic recombinant tissue plasminogen activator thrombolysis of acute stroke. *J Cereb Blood Flow Metab*. 1998;18:1298–1307.
 37. Hallenbeck JM. The many faces of tumor necrosis factor in stroke. *Nat Med*. 2002;8:1363–1368.
 38. Salomone S, Potts EM, Tyndall S, Ip PC, Chun J, Brinkmann V, Waerber C. Analysis of sphingosine 1-phosphate receptors involved in constriction of isolated cerebral arteries with receptor null mice and pharmacological tools. *Br J Pharmacol*. 2008;153:140–147.
 39. Mann DL, McMurray JJ, Packer M, Swedberg K, Borer JS, Colucci WS, Djian J, Drexler H, Feldman A, Kober L, Krum H, Liu P, Nieminen M, Tavazzi L, van Veldhuisen DJ, Waldenstrom A, Warren M, Westheim A, Zannad F, Fleming T. Targeted anticytokine therapy in patients with chronic heart failure: results of the Randomized Etorcept Worldwide Evaluation (RENEWAL). *Circulation*. 2004;109:1594–1602.

CLINICAL PERSPECTIVE

This study presents a novel concept, in which the cause of reduced cerebral blood flow in heart failure lies in the tumor necrosis factor- α - and sphingosine-1-phosphate-dependent recruitment of proximal cerebral arteries into the myogenic mechanism. Our investigation further identifies this pathophysiology as a therapeutic target. We illustrate that myogenic recruitment and consequent reductions in cerebral blood flow are reversed by tumor necrosis factor- α sequestration with etanercept, with additional benefits in cardiac function and peripheral resistance. These results challenge the notion that etanercept possesses limited usefulness for the treatment of heart failure and encourages a reevaluation using vascular and hemodynamic end points.

Supplemental Material

SUPPLEMENTAL METHODS

Reagents

Sphingosine-1-phosphate (S1P) was purchased from Biomol International (Plymouth Landing, USA), JTE013 from Tocris Bioscience (Ellisville, USA) and etanercept from Amgen (Thousand Oaks, USA). All other reagents were purchased from Sigma-Aldrich (St. Louis, USA). MOPS-buffered salt solution contained [mmol/L]: NaCl 145, KCl 4.7, CaCl₂ 3.0, MgSO₄ •7H₂O 1.17, NaH₂PO₄ •2H₂O 1.2, pyruvate 2.0, EDTA 0.02, MOPS (3-morpholinopropanesulfonic acid) 3.0, and glucose 5.0.

Animal models:

This investigation conforms to the *Guide for the Care and Use of Laboratory Animals* published by the NIH (Publication No. 85-23, revised 1996). All animal care and experimental protocols were approved by the Institutional Animal Care and Use Committees at the University of Toronto and the University Health Network (UHN), Toronto and conducted in accordance with Canadian animal protection laws.

Wild-type male mice (2-3 months; C57BL/6N) and female gerbils (2-3 months) were purchased from Charles River Laboratories (Montreal, Canada). *Sphk1*^{-/-} ¹, *Sphk2*^{-/-} ², *Sphk1*^{-/-}/*Sphk2*^{+/-} ³ and *SIP2R*^{-/-} ⁴ mice have been previously characterized and were generously provided by Dr. Richard L. Proia, Bethesda, MD. All mice were housed under a standard 12h:12h light-dark cycle, fed normal chow and had access to water *ad libitum*.

Small artery studies:

All functional vessel experiments were conducted in MOPS-buffered saline at 37°C and transmural pressure of 45mmHg, with the exception of myogenic responses (see below). *Vasomotor responses* to phenylephrine (PE; 5µmol/L) and acetylcholine (ACh; 10µmol/L) provided an assessment of vessel viability at the beginning and end of each experiment. PCAs failing to show ≥25% constriction to PE and ≥20% dilation to ACh (in the presence of 5µmol/L PE) were excluded.

Myogenic responses were elicited by step-wise 20mmHg increases in transmural pressure from 20 to 100mmHg. At each pressure step, vessel diameter (dia_{active}) was measured once a steady state was reached (5min). Vessels requiring treatment (50pg/ml TNFα, 30nmol/L S1P, 1µmol/L JTE013, or 10µg/ml etanercept) were incubated with the reagent in MOPS for 30 min at 45mmHg, and myogenic responses were then assessed in the presence of that reagent. Following completion of all dia_{active} measurements, MOPS buffer was replaced with a Ca²⁺-free version and maximal passive diameter (dia_{max}) was recorded at each pressure step. A representative data trace is provided in **Supplementary Fig. 1**.

The longitudinal gradient of myogenic activity (i.e., weak myogenic activity in proximal vs. strong activity in distal PCAs; **Figure 2A**) was studied utilizing gerbil PCAs, since distal segments of the mouse PCA branch too frequently (i.e., mouse PCA segments are too short to be cannulated without damaging them). The fact that proximal mouse and gerbil PCAs possess virtually identical diameters, responses to phenylephrine and myogenic tone, however, minimizes the concern in extrapolating the gerbil distal PCA results.

RT-PCR

RNA from PCAs was isolated using a Qiagen (Mississauga, ON) RNeasy[®] Kit, as per instructions. Standard methods were used to prepare cDNA and perform subsequent PCRs, consisting of 40 cycles of 30s denaturation (95°C); 45s primer-specific annealing; and 45s primer extension (68°C). Resultant PCR products were separated on a 2.5% agarose gel containing ethidium bromide and analyzed by densitometry with Image J software.

The primers employed in the present study included: GADPH, Forward: 5'-TTCACCACCATGGAGAAGG, Reverse: 5'-CTCGTGGTTCACACCCATC (amplicon: 111bp; annealing: 55°C) and TNF α , Forward: 5'-GGGACAGTGACCTGGACTGT, Reverse: 5'-CTCCCTTTGCAGAACTCAGG (amplicon: 111bp; annealing: 56°C)

Fluorescent co-immunolabeling

Sham-operated and heart-failure (HF, 4-6 wks post-MI) C57Bl/6 mice were anesthetized by isoflurane, and perfusion fixed transcardially with ice-cold PBS followed by 4% buffered paraformaldehyde (pH 7.4). Brains were dissected immediately and maintained in the same fixative overnight at 4°C. Caudal brain slices including the PCA were incubated in 30% sucrose overnight at 4°C for cryoprotection and embedded in OCT on isopentane and dry ice. Samples from 6-day post-MI hearts and sham-operated controls served as positive and negative controls respectively for TNF α labeling, respectively (data not shown). Cryostat sections (7 μ m for brains, 5 μ m for hearts) were collected on superfrost plus-coated slides (Fisher Scientific) and stored at -20°C. Frozen sections were air dried and washed in PBS extensively. Following 2 h pre-incubation in blocking solution of 0.1% Triton X-100, 5% donkey serum in phosphate buffered saline (PBS), sections were incubated overnight at 4°C in a humidified chamber for labeling with mouse monoclonal anti- α -actinin (for cardiac myocytes, 1:500, Sigma), anti-SM α -actin (for vascular smooth muscle cells, 1:500, Sigma), or goat anti-mouse TNF α (1:40, R&D systems). Secondary antibodies were Cy3-tagged donkey anti-mouse, Cy2-conjugated donkey anti-rabbit, and Cy5-conjugated donkey anti-goat (Jackson Immunoresearch). Hoechst nuclear stain (Molecular Probes) was added to the secondary antibody cocktail for 1h at room temperature. Omission of primary antibodies served as staining control. Samples were mounted in PBS-glycerol (1:1) solution and sealed. Images were captured with an Olympus Fluoview 1000 confocal microscope and overlaid using adobe Photoshop.

Histological analysis of infarct size:

As previously described^{5,6}, we utilized a standard, length-based measure of infarct size⁷ adapted from the method originally described by Pfeffer and co-workers⁸. Following transcardiac perfusion with 4% ice-cold paraformaldehyde, hearts were removed and post-fixed in the same fixative for at least 48 hours (at 4°C) and then paraffin embedded. Sections (5 μ m thick; cut apex to base in 200 μ m intervals) were stained with hematoxylin and eosin stain. Images of the stained sections were obtained with a Leica DMLB microscope equipped with a Photometrics Cool-Snap digital camera (Carsen Group) and analyzed with Image J software (National Institutes of Health, USA). Infarct and left ventricular circumference was measured along the epicardial surface. Infarct size (%) was calculated as the mean percentage of infarct circumference relative to the total left ventricular circumference [(infarct length / left ventricular length) x 100] over 10 serial slices.

MRI-based measurement of brain perfusion:

The FAIR technique⁹ was used to evaluate brain perfusion with a 7 Tesla micro-MRI system (BioSpec 70/30 USR, Bruker BioSpin, Ettlingen, Germany), including the B-GA12 gradient insert, 72mm inner diameter linear volume resonator for RF transmission, and anteriorly placed head coil for RF reception. FAIR isolates perfusion as an accelerated T₁ signal relaxation following slice-selective compared to non-selective inversion preparation, as per the following equation: $CBF = \lambda (1/T_{1,ss} - 1/T_{1,ns})$ (ml/(100g*min), where 'ss' and 'ns' denote slice-selective and non-selective measurements and λ is the blood-brain partition coefficient, defined as the ratio between water concentration per g brain tissue and per ml blood. This coefficient is approximately 90ml/100g in mice¹⁰.

FAIR optimization used in our study was a single-shot EPI technique with preceding adiabatic inversion. Parameters included echo time of 11ms, repetition time of 17s, 18 inversion times ranging from 25-to-6825ms in 400ms increments, 3mm slice-selective inversion slab, 16.8x16.8mm field-of-view with 64x64 matrix for 263 μ m in-plane resolution, 1mm slice thickness, and 10min 12s data acquisition time. Acquisitions were repeated in fore, middle, and hind-brain vertical sections, corresponding to anterior, mixed, and posterior circulations.

FAIR images were evaluated by manual prescription (MIPAV, NIH, Bethesda, MD; <http://mipav.cit.nih.gov>) of sub-hemispheric regions-of-interest (ROIs), termed 'global', and local ROIs corresponding to cortical and sub-cortical parenchyma in fore-brain sections; cortical and paraventricular parenchyma in middle sections; and cortical and mid-brain parenchyma in hind-brain sections. ROIs were drawn directly on T₁-weighted signal images to enable manual correction for intra-scan motion. ROIs were registered with parametric CBF maps to verify absence of bias from high perfusion vessels and meninges. T₁ regressions and CBF calculations were performed using Matlab (Mathworks, Natick, MA). Significance was defined by 1-tailed Student's t-test (P<0.05).

High resolution MRI of brain structure

Preparation of samples: We employed a previously published procedure with minor modifications¹¹. Mice were anesthetized with Ketamine (150mg/kg) and Xylazine (10mg/kg) ip. Thoracic cavities were opened, and animals were perfused through the LV with 30ml PBS (pH 7.4) containing 2mM ProHance® (gadoteridol, Bracco Diagnostics Inc., Princeton, NJ) contrast agent solution at room temperature at a rate of ~1.0 ml/min. This was followed by infusion with 30ml of 4% paraformaldehyde (PFA) at room temperature in PBS containing 2mM ProHance® at the same rate. Following perfusion, heads were removed along with skin, lower jaw, ears and cartilaginous nose tip. Remaining skull structures were allowed to postfix in 4% PFA containing 2mM ProHance® at 4°C for 12 h. Skulls were transferred to PBS with 0.02% sodium azide and 2 mM ProHance® at 4°C and rotated until scanned.

MRI acquisition: Samples were removed from contrast solution, blotted and placed into 13mm diameter plastic tubes filled with proton-free susceptibility-matching fluid (Fluorinert FC-77, 3M Corp., St. Paul, MN). A multi-channel 7.0 Tesla MRI scanner (Varian Inc., Palo Alto, CA) with a 6-cm inner bore diameter insert gradient set was used to acquire anatomical images of brains within skulls. Three custom-built 14mm diameter solenoid coils (length 18.3mm), were used to image 3 brains in parallel. Parameters used were optimized for grey/white matter contrast: a T₂-weighted,

3D fast spin-echo sequence, with TR/TE=325/32 ms, four averages, field-of-view 14×14×25 mm and matrix size 432×432×780 giving an image with 32µm isotropic voxels. Total imaging time was 11.3 h.

Image processing: The T₂-weighted MRI scans were then non-linearly aligned to a 3D atlas of the mouse brain with 62 structures identified¹². This process consisted of an initial step in which all of the MRI scans were non-linearly aligned to each other using an unbiased group wise registration algorithm¹³. Briefly, rigid body registration was carried out towards a preexisting image based on the same mouse strain. All possible pair-wise 12-parameter registrations were then carried out to create an unbiased linear average model of the entire data set. All images were subsequently non-linearly aligned towards the 12-parameter average. The resulting registered MRIs were re-sampled and averaged^{13,14}. This iterative procedure was repeated for an additional 5 generations with even finer deformation grid-point spacing. The end-result is to have all scans deformed into exact alignment with each other in an unbiased fashion. This allows for the analysis of the deformations needed to take each mouse's anatomy into this final atlas space, the goal being to model how the deformation fields relate to genotype. Correspondence with the 3D atlas was obtained by non-linear alignment of the final stage average MRI with the 40-mouse average MRI upon which the atlas is based¹².

Image analysis: Local differences in brain shape related to treatment and time point post surgery were assessed by analysis of the deformation fields^{15,16}. To reduce random noise and assure normality under the central limit theorem, the transformation data was blurred prior to analysis with a Gaussian kernel with a full-width at half max of 1mm, and the logarithm of the Jacobian was computed for univariate statistical comparison at every image point. This statistical analysis results in millions of separate statistical tests. In order to account for an inflated type I error, the False Discovery Rate (FDR) technique was applied¹⁷. The volume for each anatomical structure defined in the atlas was computed for each mouse by integrating the Jacobian of the transformation mapping the atlas image to the image for that mouse. This procedure has previously been shown to provide volume estimates comparable to those obtained by standard stereological methods using tissue sections¹⁸. The homogeneity of variance in the volumes of the anatomical structures was tested using the Fligner-Killeen test.

Morris water maze:

This cognitive test was conducted as described¹⁹. Mice were placed in a circular pool (1.54m diameter) of opaque water (22°C) with a hidden platform (20cm diameter) 2cm below the water surface. The mice were allowed to swim until they found and climbed onto the hidden platform. Unique shapes and cues were arrayed around the pool, so that, with repetition, the mice are able to learn the location of the hidden platform. Mice initially underwent a training procedure to acclimatize them to the test room and pool. Subsequently, mice were tested over 5 consecutive days with 2 sessions per day at 0900h and 1300h (10 sessions overall). Acquisition was assessed during sessions 1-6, where the platform was maintained in “quadrant 1”. At session 7, the platform was moved to “quadrant 3” for testing of reverse learning, and remained in quadrant 3 until session 10. The first 30s of session 7 were analyzed as a probe trial, where the time spent swimming in the quadrant where the platform had previously been located (quadrant 1) was measured. A probe trial is the most specific form of assessment of spatial memory. The latency to find the platform, the swim speed and path of the mouse during each trial was recorded by a video camera

suspended above the centre of the pool and connected to a video tracking system (HVS Image Advanced Tracker VP200, HVS Image, Buckingham, UK). The swim path for each trial was automatically plotted in the HVS image system and the search strategies to the trial of each session were analyzed using a categorization scheme based on the method described by Brody²⁰. Strategies were classified into 3 broad categories: spatial, systematic but non-spatial and repetitive looping path.

Statistical analysis of supplemental data:

All supplemental data are expressed as means \pm SEM, where n is the number of vessels or animals studied. An unpaired Student's t test was utilized for the comparison of two separate groups (e.g., sham vs. HF). Where appropriate (e.g. pre- and post-inhibitor), a paired Student's t test was employed. For comparison of multiple groups, an ANOVA followed by t tests with Bonferroni correction was used. Differences were considered significant at $P < 0.05$.

SUPPLEMENTAL TABLE 1a) S1P-induced enhancement of myogenic tone in *mouse PCAs*:

transmural pressure (mmHg)	control (% of dia _{max})	+ S1P (% of dia _{max})	P value
45	4.1±2.0	10.6±2.6	<0.05
20	3.0±0.9	6.7±2.0	<0.05
40	4.8±2.3	11.7±3.0	<0.05
60	4.6±1.5	10.2±2.4	<0.05
80	4.0±0.8	7.8±1.7	<0.05
100	3.0±0.5	6.0±1.2	<0.05

b) S1P-induced enhancement of myogenic tone in *gerbil PCAs*:

transmural pressure (mmHg)	control (% of dia _{max})	+ S1P (% of dia _{max})	P value
45	7.5±2.9	17.6±2.6	<0.05
20	3.7±0.7	10.1±1.4	<0.05
40	5.4±1.7	13.9±2.2	<0.05
60	9.3±2.8	18.0±2.4	<0.05
80	13.3±3.3	19.7±2.8	<0.05
100	15.6±3.4	20.8±3.0	NS

Enhancement of myogenic tone by S1P:

Proximal PCAs from (a) mice and (b) gerbils were exposed to increasing transmural pressures (20- to-100mmHg in 20mmHg increments). In PCAs from both species, myogenic tone was markedly increased in the presence of a low concentration of sphingosine-1-phosphate (S1P, 10nmol/L, p<0.05, n=6 for both species).

SUPPLEMENTAL TABLE 2

Comparison of hemodynamic parameters in Sphk1 knockout sham and heart failure mice at 6 weeks post-LAD ligation

OP/treatment	units	Sphk1^{-/-} sham	Sphk1^{-/-} HF
body weight	g	29.9±1.7	26.3±2.9
heart weight	mg	206±18	242±40
heart/body weight ratio	mg/g	6.5±0.3	9.4±1.2*
lung weight	mg	159±15	171±17
liver weight	mg	1335±149	1179±103
heart rate	min ⁻¹	322±26	306±7
LVEF	%	84.7±1.1	61.1±1.7*
SP	mmHg	89±5	91±8
DP	mmHg	53±4	62±8
stroke volume	μl	181±24	92±7*
MAP	mmHg	65±4	72±8
CO	ml/min	5.5±0.4	2.8±0.2*
TPR	mmHg*min /ml	11.9±0.6	26.6±3.3*

Data are mean±SEM. *P<0.05 for unpaired comparisons; n=8 for both groups.

Acronyms: LVEF – Left ventricular ejection fraction; SP – Systolic pressure; DP – Diastolic pressure; MAP – mean arterial pressure; CO - cardiac output; TPR – total peripheral resistance; CBF – global cerebral blood flow.

Mortality rates were 0% for the sham and LAD-ligation procedures, respectively.

SUPPLEMENTAL TABLE 3

Comparison of hemodynamic parameters in sham mice, heart failure mice and heart failure mice treated with etanercept at 2 WEEKS post-LAD ligation

OP/treatment	units	sham / saline	HF / saline	HF / ETN	n
body weight	g	23.9±1.2	23.8±0.8	24.9±1.5	10
heart weight	mg	119±4	179±13*	149±5* [#]	10
infarct size	%	--	22±4	16±4	7
heart/body weight ratio	mg/g	5.1±0.1	7.5±0.3*	6.1±0.2*	10
lung weight	mg	154±5	195±14*	162±9	10
liver weight	mg	994±111	1179±27*	1077±49	10
heart rate	min ⁻¹	298±13	297±15	342±9	8
LVEF	%	73.5±2.2	47.3±1.6*	62.1±1.5* [#]	8
LVESP	mmHg	117±2	106±1*	107±4	8
LVEDP	mmHg	2.3±0.6	10.6±2.3*	6.2±1.1	8
stroke volume	μl	226±25	101±18*	146±12*	8
MAP	mmHg	92±4	78±8*	86±8	8
CO	ml/min	6.6±0.6	3.2±0.4*	4.9±0.3 [#]	8
TPR	mmHg*min/ml	14.8±1.4	27.8±3.4*	17.9±1.4 [#]	8
CBF	ml/100g*min	220±8	189±7*	228±5 [#]	7-8

Data are mean±SEM. *P<0.05 unpaired, multiple comparisons to sham-operated and saline-treated (sham/saline) mice; #P<0.05 unpaired, multiple comparisons to HF saline-treated (HF/saline)

Acronyms: LVEF – Left ventricular ejection fraction; LVESP – Left ventricular end systolic pressure; LVEDP – Left ventricular end diastolic pressure; MAP – mean arterial pressure; CO - cardiac output; TPR – total peripheral resistance; CBF – global cerebral blood flow.

Mortality rates were 0% and 17% for the sham and LAD-ligation procedures, respectively. All mortality in HF mice was observed within 5 days of LAD-ligation (i.e., before randomization into the saline or etanercept treatment group).

SUPPLEMENTAL TABLE 4

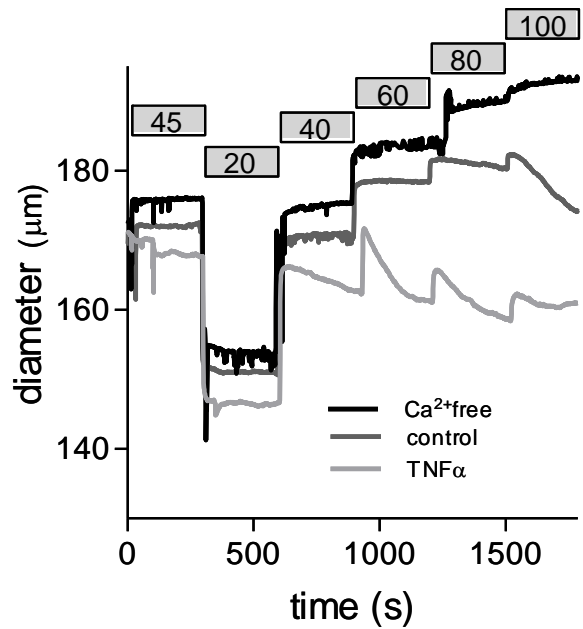
Comparison of hemodynamic parameters in sham mice, heart failure mice and heart failure mice treated with etanercept at 6 WEEKS post-LAD ligation

OP/treatment	units	sham / saline	HF / saline	HF / ETN	n=
body weight	g	27.9±1.4	26.1±1.2	26.0±1.1	14
heart weight	mg	152±10	197±12*	188±16	14
infarct size	%	--	25±4	23±5	8
heart/body weight ratio	mg/g	5.8±0.2	7.6±0.4*	7.2±0.5*	14
lung weight	mg	146±7	185±9*	163±10	14
liver weight	mg	1273±119	1244±71	1179±71	14
heart rate	min ⁻¹	362±10	302±16	380±26 [#]	8
LVEF	%	77.0±3.7	48.4±1.8*	51.9±2.4*	8
LVESP	mmHg	125±1	110±2*	122±2 [#]	8
LVEDP	mmHg	2.8±0.5	5.9±1.6*	2.4±0.2 [#]	8
stroke volume	μl	195±18	113±11*	92±11*	8
MAP	mmHg	90±3	79±1*	89±2 [#]	8
CO	ml/min	5.3±0.3	3.6±0.5*	3.4±0.4	8
TPR	mmHg*min/ml	13.2±0.7	26.2±3.3*	28.3±3.2*	8

Data are mean±SEM. *P<0.05 unpaired, multiple comparisons to sham-operated and saline-treated (sham/saline) mice; #P<0.05 unpaired, multiple comparisons to HF saline-treated (HF/saline)

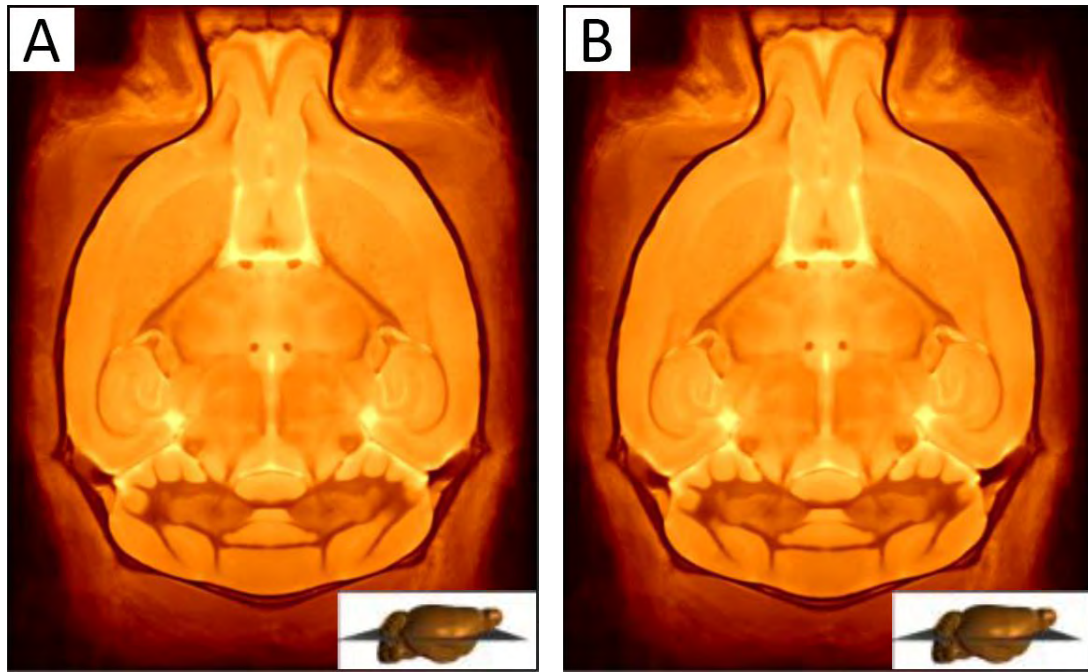
Acronyms: LVEF – Left ventricular ejection fraction; LVESP – Left ventricular end systolic pressure; LVEDP – Left ventricular end diastolic pressure; MAP – mean arterial pressure; CO - cardiac output; TPR – total peripheral resistance.

Mortality rates were 4% and 19% for the sham and LAD-ligation procedures, respectively. All mortality was observed within 5 days of sham or LAD-ligation procedure (i.e., before randomization into the saline or etanercept treatment group).



Representative tracings of myogenic responses

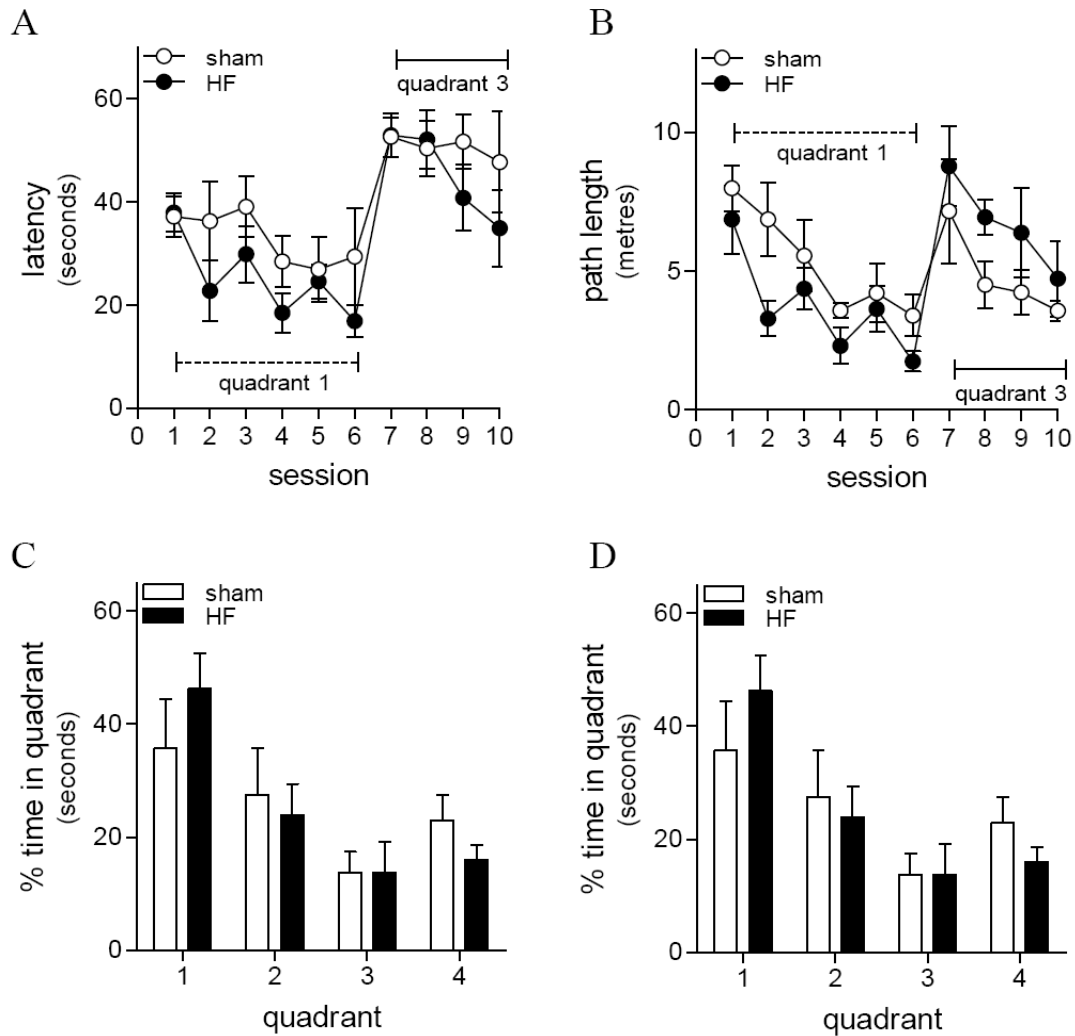
Stepwise increases in transmural pressure (20-100mmHg) are indicated in the boxes above the tracing. The control tracing (dark gray) is acquired first. If treatment is necessary, the vessel is treated for 30min at 45mmHg and the assessment protocol is repeated. In this figure, the vessel was treated with 50pg/ml TNF α (light gray tracing). Accordingly, in this experiment, the two gray tracings shown (control, TNF α) represent “dia_{active}” measurements. Upon completion of myogenic assessments, MOPS buffer is replaced with a Ca²⁺-free buffer and the final assessment of passive vessel diameters (dia_{max}) is performed (black tracing).



Early stage heart failure does not affect brain anatomy

The deformation fields needed to align brains to a consensus average brain can be used to determine tissue expansion or contraction^{21,22}. This allows for the analysis of regional differences in the tissue volume and shape of brains from **(A)** mice with heart failure (HF; 6 wks post-LAD ligation) and **(B)** sham-operated controls. Since HF may cause heterogeneous effects, local differences in brain shape and image intensity between individual HF mice and their respective sham-operated control group were assessed. A test of homogeneity of variance in the volumes of the anatomical structures was applied. No significant differences in overall brain size and shape were assessed by this procedure (n=4). Additionally, none of the following structures were altered by HF: amygdala, arbor vita of cerebellum, basal forebrain, cerebellar cortex, cerebral cortex: entorhinal cortex, cerebral cortex: frontal lobe, cerebral cortex: occipital lobe, cerebral cortex: parieto-temporal lobe, colliculus inferior, colliculus superior, corpus callosum, dentate gyrus of the hippocampus, hippocampus, hypothalamus, medulla, midbrain, nucleus accumbens, olfactory bulbs, olfactory tubercle, periaqueductal grey, pons, striatum, and thalamus.

SUPPLEMENTAL FIGURE 3

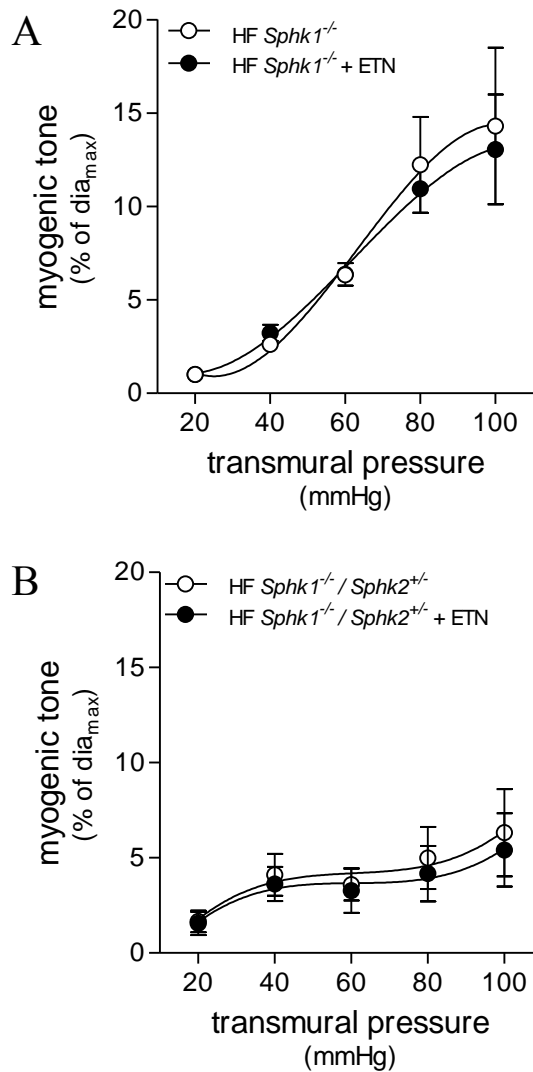


Heart failure for 6 wks does not affect learning behavior or spatial memory in mice

Using the *Morris water maze test*¹⁹, no differences were observed between mice with heart failure (HF; 6 wks post-LAD ligation) and sham-operated controls in terms of (A) latency (the time to find the platform) or (B) path length (distance swam to find the platform) in sessions 1-6. The % time spent in quadrant 1 during session 6 (C) indicated that both experimental groups showed a preference for quadrant 1, with no differences observed between HF and sham controls.

The platform was moved to quadrant 3 for sessions 7-10 (a test of spatial memory and reverse learning), which increased both latency and path length (since the mice need re-learn the location of the hidden platform). The % time spent in quadrant 1 during session 7 (D) indicated that both experimental groups continued to show a preference for quadrant 1 at the beginning of the re-learning task, with no differences observed between HF and sham controls. For both groups, n=4; comparisons were only between the sham and HF group within each session (panels A/B) or quadrant (panels C/D).

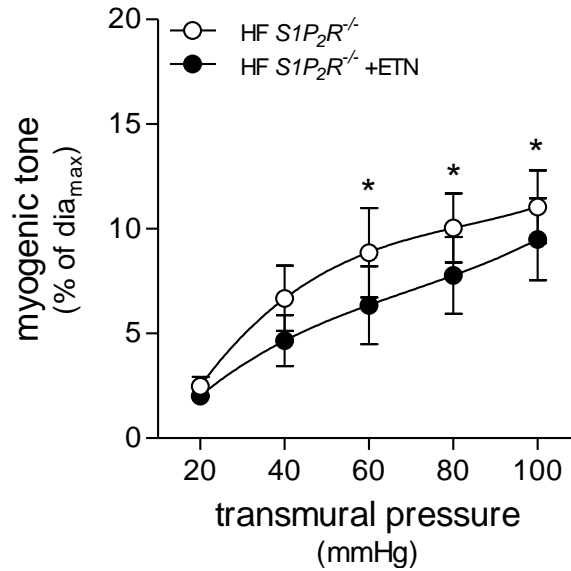
SUPPLEMENTAL FIGURE 4



Etanercept has no effect on PCAs isolated from heart failure mice lacking Sphk1

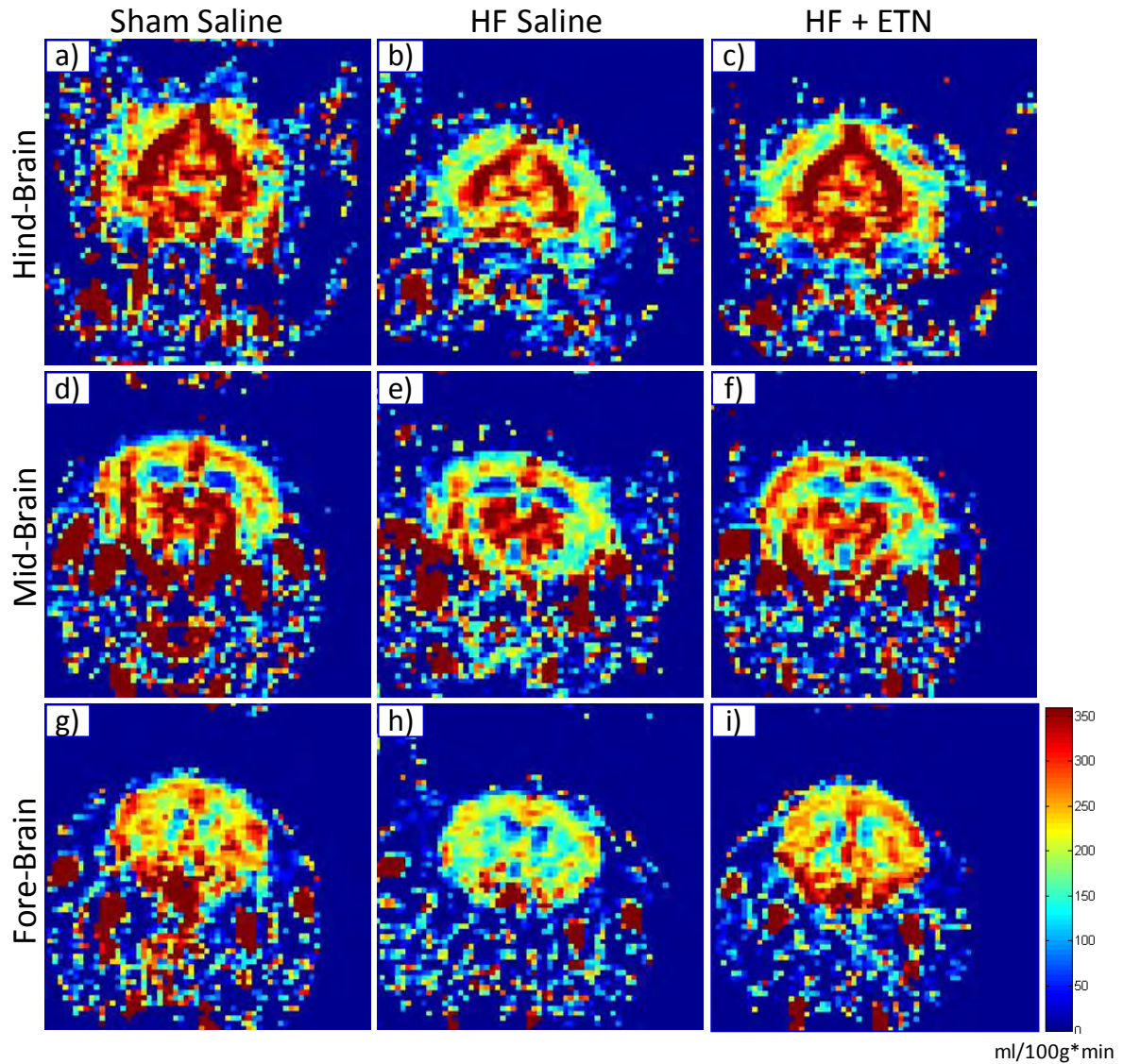
The TNF α antagonist etanercept (ETN) did not alter myogenic tone in PCAs isolated from HF mice (4-6 wks post-MI) lacking *Sphk1* (**A**: *Sphk1*^{-/-}; n=3 paired comparisons) or HF mice (4-6 wks post-MI) lacking *Sphk1* and one allele of *Sphk2* (**B**: *Sphk1*^{-/-} / *Sphk2*^{+/-}; n=6 paired comparisons).

SUPPLEMENTAL FIGURE 5



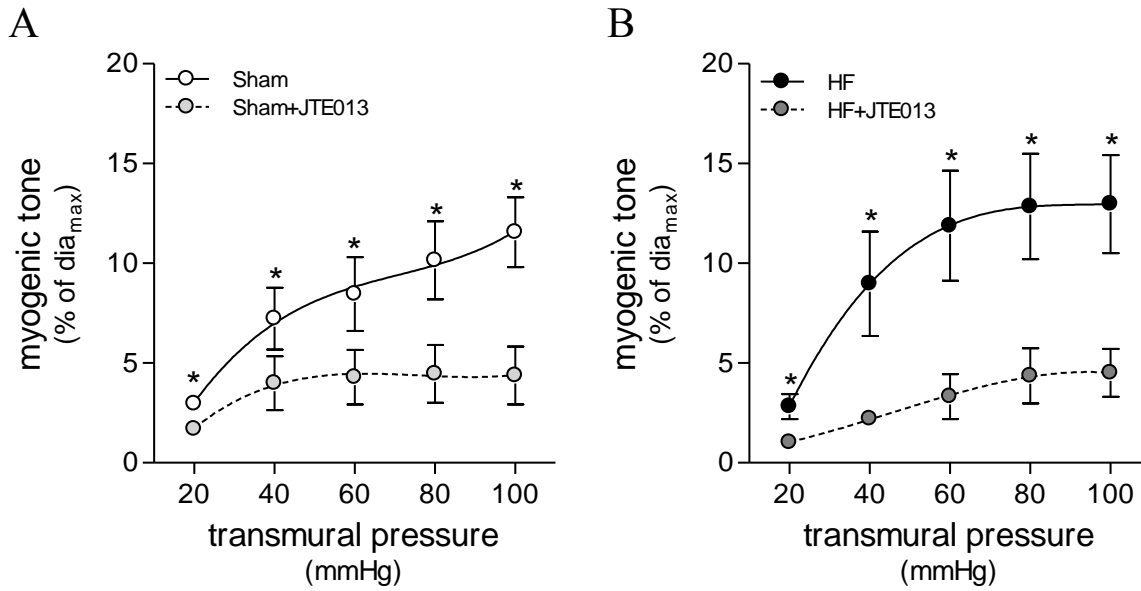
Etanercept has no effect on PCAs from mice lacking $Sphk1$ or $S1P_2R$

In PCAs isolated from HF mice (4-6 wks post-MI) lacking the $S1P_2$ receptor ($S1P_2R^{-/-}$; n=6), etanercept (ETN) stimulated a small but significant reduction in myogenic tone at transmurial pressures ≥ 60 mmHg. *P<0.05 for paired comparisons.



Etanercept treatment improves cerebral blood flow in mice with heart failure

Shown are representative FAIR-Magnetic Resonance Images assessing blood flow fore-brain (**a-c**), mid-brain (**d-f**) and hind-brain (**g-i**). Blood flow was reduced in all regions during heart failure (**b,e,h**), compared to sham controls (**a,d,g**). Etanercept mitigated these reductions in blood flow (**c,f,i**). The images are representative of 28 separate experiments for sham animals, 30 for heart failure animals and 8 etanercept-treated animals.



JTE013 attenuates myogenic tone in PCAs isolated from S1P₂R knockout mice

JTE013 (1µmol/L, 30min) attenuated myogenic vasoconstriction in PCAs isolated S1P₂ receptor knockout mice under both **(A)** sham-operated (n=5) and **(B)** heart failure (HF; n=6) conditions. *P<0.05 for paired comparisons.

SUPPLEMENTAL REFERENCES

1. Allende ML, Sasaki T, Kawai H, Olivera A, Mi Y, Echten-Deckert G, Hajdu R, Rosenbach M, Keohane CA, Mandala S, Spiegel S, Proia RL. Mice deficient in sphingosine kinase 1 are rendered lymphopenic by FTY720. *J Biol Chem.* 2004; 279:52487-52492.
2. Mizugishi K, Yamashita T, Olivera A, Miller GF, Spiegel S, Proia RL. Essential role for sphingosine kinases in neural and vascular development. *Mol Cell Biol.* 2005; 25:11113-11121.
3. Mizugishi K, Li C, Olivera A, Bielawski J, Bielawska A, Deng CX, Proia RL. Maternal disturbance in activated sphingolipid metabolism causes pregnancy loss in mice. *J Clin Invest.* 2007; 117:2993-3006.
4. Kono M, Mi Y, Liu Y, Sasaki T, Allende ML, Wu YP, Yamashita T, Proia RL. The sphingosine-1-phosphate receptors S1P1, S1P2, and S1P3 function coordinately during embryonic angiogenesis. *J Biol Chem.* 2004; 279:29367-29373.
5. Noyan-Ashraf MH, Momen MA, Ban K, Sadi AM, Zhou YQ, Riazi AM, Baggio LL, Henkelman RM, Husain M, Drucker DJ. GLP-1R agonist liraglutide activates cytoprotective pathways and improves outcomes after experimental myocardial infarction in mice. *Diabetes.* 2009; 58:975-983.
6. Hoefler J, Azam MA, Kroetsch JT, Poi HL, Momen MA, Voigtlaender-Bolz J, Scherer EQ, Meissner A, Bolz SS, Husain M. Sphingosine-1-Phosphate-Dependent Activation of p38 MAPK Maintains Elevated Peripheral Resistance in Heart Failure Through Increased Myogenic Vasoconstriction. *Circ Res.* 2010; 107:923-933.
7. Takagawa J, Zhang Y, Wong ML, Sievers RE, Kapasi NK, Wang Y, Yeghiazarians Y, Lee RJ, Grossman W, Springer ML. Myocardial infarct size measurement in the mouse chronic infarction model: comparison of area- and length-based approaches. *J Appl Physiol.* 2007; 102:2104-2111.
8. Pfeffer MA, Pfeffer JM, Fishbein MC, Fletcher PJ, Spadaro J, Kloner RA, Braunwald E. Myocardial infarct size and ventricular function in rats. *Circ Res.* 1979; 44:503-512.
9. Kim SG. Quantification of relative cerebral blood flow change by flow-sensitive alternating inversion recovery (FAIR) technique: application to functional mapping. *Magn Reson Med.* 1995; 34:293-301.
10. Herscovitch P, Raichle ME. What is the correct value for the brain--blood partition coefficient for water? *J Cereb Blood Flow Metab.* 1985; 5:65-69.
11. Tyszka JM, Readhead C, Bearer EL, Pautler RG, Jacobs RE. Statistical diffusion tensor histology reveals regional dysmyelination effects in the shiverer mouse mutant. *Neuroimage.* 2006; 29:1058-1065.
12. Dorr AE, Lerch JP, Spring S, Kabani N, Henkelman RM. High resolution three-dimensional brain atlas using an average magnetic resonance image of 40 adult C57Bl/6J mice. *Neuroimage.* 2008; 42:60-69.
13. Kovacevic N, Henderson JT, Chan E, Lifshitz N, Bishop J, Evans AC, Henkelman RM, Chen XJ. A three-dimensional MRI atlas of the mouse brain with estimates of the average and variability. *Cereb Cortex.* 2005; 15:639-645.
14. Collins DL, Neelin P, Peters TM, Evans AC. Automatic 3D intersubject registration of MR volumetric data in standardized Talairach space. *J Comput Assist Tomogr.* 1994; 18:192-205.

15. Gaser C, Volz HP, Kiebel S, Riehemann S, Sauer H. Detecting structural changes in whole brain based on nonlinear deformations-application to schizophrenia research. *Neuroimage*. 1999; 10:107-113.
16. Nieman BJ, Flenniken AM, Adamson SL, Henkelman RM, Sled JG. Anatomical phenotyping in the brain and skull of a mutant mouse by magnetic resonance imaging and computed tomography. *Physiol Genomics*. 2006; 24:154-162.
17. Genovese C, Wasserman L. Operating characteristics and extensions of the false discovery rate procedure. *Journal of the Royal Statistical Society Series B-Statistical Methodology*. 2002; 64:499-517.
18. Lerch JP, Carroll JB, Dorr A, Spring S, Evans AC, Hayden MR, Sled JG, Henkelman RM. Cortical thickness measured from MRI in the YAC128 mouse model of Huntington's disease. *Neuroimage*. 2008; 41:243-251.
19. Kapoor A, Kostaki A, Janus C, Matthews SG. The effects of prenatal stress on learning in adult offspring is dependent on the timing of the stressor. *Behav Brain Res*. 2009; 197:144-149.
20. Brody DL, Holtzman DM. Morris water maze search strategy analysis in PDAPP mice before and after experimental traumatic brain injury. *Exp Neurol*. 2006; 197:330-340.
21. Gaser C, Volz HP, Kiebel S, Riehemann S, Sauer H. Detecting structural changes in whole brain based on nonlinear deformations-application to schizophrenia research. *Neuroimage*. 1999; 10:107-113.
22. Nieman BJ, Flenniken AM, Adamson SL, Henkelman RM, Sled JG. Anatomical phenotyping in the brain and skull of a mutant mouse by magnetic resonance imaging and computed tomography. *Physiol Genomics*. 2006; 24:154-162.